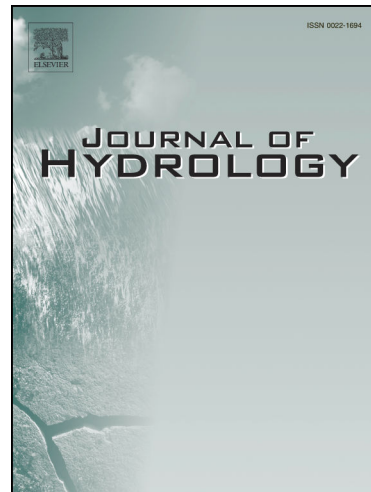


Journal Pre-proofs

Maximum Entropy Modeling to Identify Physical Drivers of Shallow Snowpack Heterogeneity using Unpiloted Aerial System (UAS) Lidar

Eunsang Cho, Adam G. Hunsaker, Jennifer M. Jacobs, Michael Palace,
Franklin B. Sullivan, Elizabeth A. Burakowski

PII: S0022-1694(21)00772-1
DOI: <https://doi.org/10.1016/j.jhydrol.2021.126722>
Reference: HYDROL 126722



To appear in: *Journal of Hydrology*

Received Date: 26 March 2021
Revised Date: 1 July 2021
Accepted Date: 20 July 2021

Please cite this article as: Cho, E., Hunsaker, A.G., Jacobs, J.M., Palace, M., Sullivan, F.B., Burakowski, E.A., Maximum Entropy Modeling to Identify Physical Drivers of Shallow Snowpack Heterogeneity using Unpiloted Aerial System (UAS) Lidar, *Journal of Hydrology* (2021), doi: <https://doi.org/10.1016/j.jhydrol.2021.126722>

This is a PDF file of an article that has undergone enhancements after acceptance, such as the addition of a cover page and metadata, and formatting for readability, but it is not yet the definitive version of record. This version will undergo additional copyediting, typesetting and review before it is published in its final form, but we are providing this version to give early visibility of the article. Please note that, during the production process, errors may be discovered which could affect the content, and all legal disclaimers that apply to the journal pertain.

© 2021 Elsevier B.V. All rights reserved.

1 **Maximum Entropy Modeling to Identify Physical Drivers of Shallow
2 Snowpack Heterogeneity using Unpiloted Aerial System (UAS) Lidar**

5 Eunsang Cho^{1,2*}, Adam G. Hunsaker^{3,4}, Jennifer M. Jacobs^{3,4}, Michael Palace^{4,5}, Franklin B.
6 Sullivan⁴, Elizabeth A. Burakowski⁴

8 ¹Hydrological Sciences Laboratory, NASA Goddard Space Flight Center, Greenbelt, MD, USA

9 ²Earth System Science Interdisciplinary Center, University of Maryland, College Park, MD,
10 USA

11 ³Department of Civil and Environmental Engineering, University of New Hampshire, Durham,
12 NH, USA

13 ⁴Earth Systems Research Center, Institute for the Study of Earth, Oceans, and Space, University
14 of New Hampshire, Durham, NH, USA

15 ⁵Department of Earth Sciences, University of New Hampshire, Durham, NH, USA

18 *Corresponding author: Eunsang Cho (escho@umd.edu)

24 Highlights

- 25 • Drivers of snow spatial patterns from UAS lidar were identified using MaxEnt
- 26 • Plant functional type and terrain roughness are the largest contributors
- 27 • Soil properties were also important controls probably due to thermal transfer

32 1st Revision Submitted to *Journal of Hydrology*

33 July 1, 2021

35 **Abstract**

36 Understanding the spatial variability of the snowpack is valuable for hydrologists and
 37 ecologists seeking to predict hydrological processes in a cold region. Snow distribution is a
 38 function of interactions among static variables, such as terrain, vegetation, and soil properties,
 39 and dynamic meteorological variables, such as solar radiation, wind speed and direction, and soil
 40 moisture. However, identifying the dominant physical drivers responsible for spatial patterns of
 41 the snowpack, particularly for ephemeral, shallow snowpacks, has been challenged due to the
 42 lack of the high-resolution snowpack and physical variables with high vertical accuracy as well
 43 as inherent limitations in traditional approaches. This study uses an Unpiloted Aerial System
 44 (UAS) lidar-based snow depth and static variables (1-m spatial resolution) to analyze field-scale
 45 spatial structures of snow depth and apply the Maximum Entropy (MaxEnt) model to identify
 46 primary controls over open terrain and forests at the University of New Hampshire Thompson
 47 Farm Research Observatory, New Hampshire, United States. We found that, among nine
 48 topographic and soil variables, plant functional type and terrain roughness contribute up to 80%
 49 and 76% of relative importance in the MaxEnt framework to predicting locations of deeper or
 50 shallower snowpacks, respectively, across a mixed temperate forested and field landscape. Soil
 51 variables, such as organic matter and saturated hydraulic conductivity, were also important
 52 controls (up to 70% and 81%) on snow depth spatial variations for both open and forested
 53 landscapes suggesting spatial variations in soil variables under snow can control thermal transfer
 54 among soil, snowpack, and surface-atmosphere. This work contributes to improving land surface
 55 and snow models by informing parameterization of the sub-grid scale snow depths, down-scaling
 56 remotely sensed snow products, and understanding field scale snow states.

57

58 **1. Introduction**

59 Snow plays a significant role in hydrologic and ecological processes globally (Barnett et
 60 al., 2005). It also benefits much of the world's population from climate services through the
 61 retention of water for release during seasonally dry periods and land surface energy budgets
 62 (Sturm et al., 2017). Snowpack structure and evolution determine snowmelt runoff, infiltration,
 63 and groundwater recharge (Carroll et al., 2019; Earman et al., 2006; Harpold et al., 2015;
 64 Lundquist et al., 2004; Maurer and Bowling, 2014). Snow plays an important role in partitioning

65 incoming solar radiation and longwave radiation into outgoing longwave radiation, and latent
 66 heat, ground heat, and sensible heat fluxes (Ge and Gong, 2010; Lawrence and Slater, 2010;
 67 Liston, 1999; Stieglitz et al., 2001). Snow's insulating properties control the underlying soils'
 68 freeze-thaw state (Groffman et al., 2001; Starkloff et al. 2017; Yi et al. 2019) affecting soil
 69 respiration, carbon sequestration, nutrient retention, and microbial communities (Aase and
 70 Siddoway, 1979; Isard and Schaetzl, 1998; Monson et al., 2006; Henry, 2008; Aanderud et al.,
 71 2013; Tucker et al., 2016; Sorensen et al., 2018; Reinmann and Templer, 2018). In addition to
 72 the total amount of snow, the spatial nonuniformity of snow exerts a strong control on processes
 73 for patchy snow in shallow ephemeral snowpacks (Anderton et al., 2002; Lundquist and
 74 Dettinger, 2004; Schlogl et al. 2018). When interactions among terrain, vegetation, and soils and
 75 snowpack are captured, they can also be useful in parameterizing the sub-grid scale in snow
 76 models to improve model accuracy (Luce et al., 1999; Sturm and Wagner, 2010) or to downscale
 77 remotely sensed snow products (e.g., radar backscatter, passive microwave, and gamma radiation;
 78 Cho et al., 2020; Derksen et al., 2010; Lemmetyinen et al., 2016; Saberi et al., 2020) that are too
 79 coarse to provide an understanding of conditions at field scales.

80 The spatial variability in snow depth is a function of static and dynamic conditions over a
 81 range of spatial scales (Clark et al., 2011). Fixed physical controls including terrain (Blöschl and
 82 Kirnbauer, 1992; Lapen and Martz, 1996; Mott et al., 2011), vegetation (Gelfan et al., 2004;
 83 DeBeer and Pomeroy, 2010; Currier and Lundquist, 2018), and even soil (Mott et al., 2013;
 84 Shook et al., 1993; Pomeroy et al., 1998) are primary controls for variations in snow depth and
 85 snow water equivalent at multiple scales across the landscape. In the absence of major vegetation
 86 interactions, terrain elevation, slope, aspect, and roughness can control accumulation and
 87 ablation patterns, with greater accumulation at higher elevations (Grünwald and Lehning, 2011),
 88 reduced snow depth on steep slopes (Blöschl and Kirnbauer, 1992), lee slope loading with
 89 preferential wind deposition of precipitation (Mott et al. 2011), retention of snowpack on north
 90 facing slopes during the ablation season (Gray and Male, 1981; Schirmer and Pomeroy, 2020),
 91 and rougher terrain holding less snow than smoother terrain (Lehning et al., 2011). With tall
 92 vegetation, canopy interception by coniferous forests (30-79%) can reduce accumulation on the
 93 ground (McNay et al. 1988; Schmidt and Gluns, 1991; Pomeroy and Gray, 1995; Storck et al.
 94 2002; Roth and Nolin, 2017, and others), though the magnitude of canopy interception depends
 95 on storm type and canopy crown completeness. Less is known about deciduous forest canopy

96 interception, which ranges from 1% based on a hardwood forest study in Japan (Nakai et al. 1993)
 97 and up to 25% in a southern beech forest in Peru (Huerta et al. 2019). Vegetation can also affect
 98 snow spatial variability during the ablation season through canopy shading (Essery et al. 2008;
 99 Musselman et al. 2008) and reduced sublimation (Roth and Nolin, 2017). Many western U.S.
 100 studies have identified elevation and temperature as primary factors explaining differences in
 101 forested versus open snowpack accumulation and duration (Lundquist et al., 2013; Roth and
 102 Nolin, 2017). For soil-snow interactions, previous work indicates that the spatial distribution of
 103 snowpack and melt timing controlled spatial patterns in soil moisture and temperature (Shook et
 104 al., 1993; Mott et al., 2013). However, there is limited research regarding if and how soil
 105 property spatial variations contribute to snow distribution during the accumulation and ablation
 106 periods.

107 Traditional manual ground sampling methods have been used to characterize snow depth
 108 spatial variability using statistical indicators, probability distributions, and fractal methods.
 109 Using traditional point measurements with a limited sample size requires a balance between the
 110 sampling spatial extent and sample density. This impacts the ability to capture spatial variability
 111 that naturally increases with spatial scale as compared to capturing small-scale spatial structures
 112 (Clark et al. 2011). Remote sensing methods provide the ability to collect data over a continuous
 113 spatial extent, thus expanding the understanding of snow distribution (Broxton et al., 2019;
 114 Deems et al., 2006; Painter et al., 2016; Jacobs et al., 2021; Tinkham et al., 2014).

115 Over the past two decades, airborne remote sensing methods, providing spatially
 116 continuous, high-resolution snow depth maps at local and regional scales, have greatly advanced
 117 the ability to characterize the spatiotemporal heterogeneity of snow depth over earlier work using
 118 snow probes (see reviews in Deems et al., 2013; López-Moreno et al., 2017). Airborne laser
 119 scanning (ALS) (Cline et al., 2009; Deems et al., 2013; Harpold et al., 2014; Kirchner et al.,
 120 2014), terrestrial laser scanning (TLS) (Grünewald et al. 2010; Currier et al. 2019), and structure-
 121 from-motion photogrammetry (SfM) (Nolan et al., 2015; Bühler et al., 2016; Goetz and Brenning,
 122 2019) have emerged as viable methods to map surface elevations with snow-off and snow-on
 123 conditions to differentially map snow depths.

124 Many snowpack patterns are controlled by fixed physical controls including vegetation
 125 and topography that are relatively consistent from year to year (i.e., time stable; Grayson et al.
 126 2002; Pflug & Lundquist, 2020; Revuelto et al., 2014). Because these snowpack patterns repeat

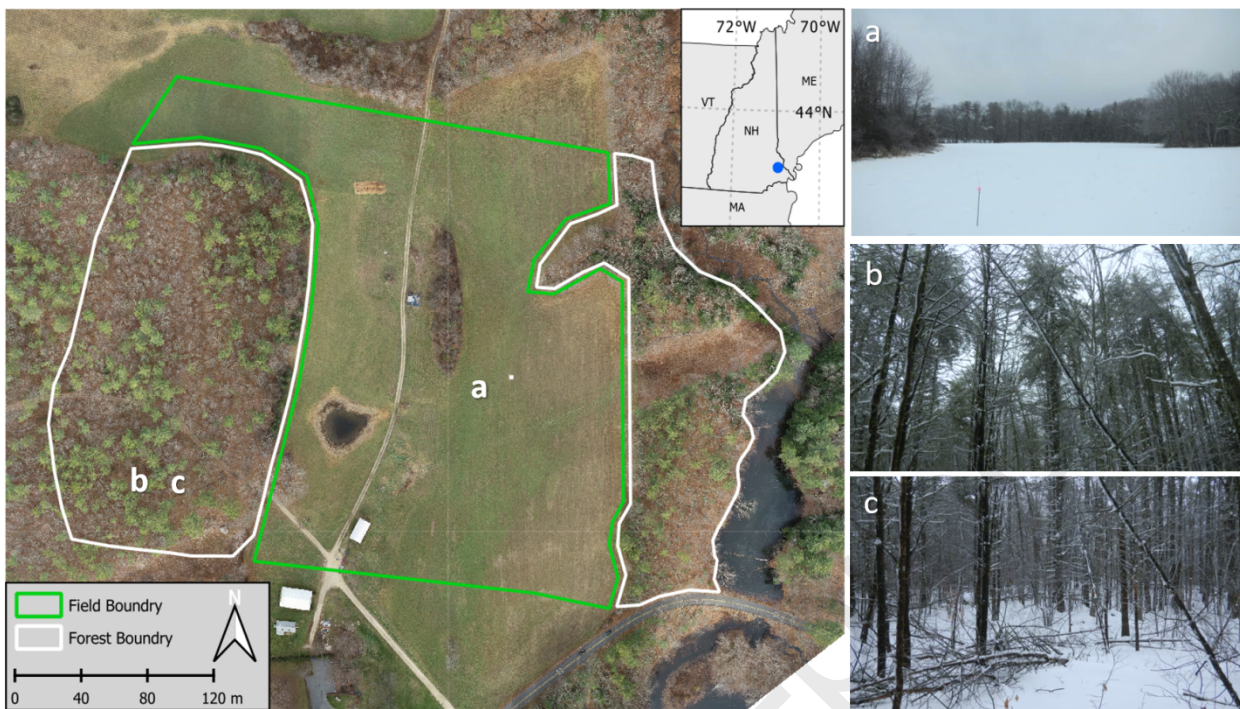
127 on an annual basis, high-resolution snow depth datasets in combination with increasingly
 128 sophisticated and ubiquitous terrain, vegetation, and soil property datasets are well suited to
 129 improve characterization of the role of fixed physical controls via data-intensive methods (e.g.,
 130 generalized linear or additive models; ensembles of regression trees such as random forests or
 131 boosted regression trees) that have been used for many purposes in hydrology and ecology
 132 (Booker and Woods, 2014; Cutler et al., 2007; He et al., 2016; López-Moreno & Nogués-Bravo,
 133 2005; Tinkham et al., 2014; Peters et al., 2007). One such spatial modeling technique that has not
 134 been used to study snow depth patterns is the Maximum Entropy (MaxEnt) model. The MaxEnt
 135 in combination with high-resolution remote sensing techniques has the potential to characterize
 136 the role of multiple physical variables simultaneously on snow depth spatial variability as well as
 137 their relative importance.

138 MaxEnt is a machine learning approach that uses the spatial location of focal features and
 139 predictor variables to extrapolate these features across a landscape where those predictor
 140 variables are present (Baldwin, 2009; Phillips et al., 2004; 2006; Phillips & Dudík, 2008). In the
 141 ecological science community, the MaxEnt model has been successfully utilized for species
 142 distribution modeling with numerous applications (Elith et al., 2006; Phillips & Dudík, 2008;
 143 Merow et al., 2013, Algeo et al., 2017). Using the MaxEnt model, ecologists predicted habitat
 144 suitability of animal and plant species using related spatial-environmental factors as predictor
 145 variables (Dudík et al., 2007). The principle of the MaxEnt model originates in information
 146 theory (Jaynes, 1957), but its application has been expanded to various disciplines, such as
 147 archaeology (Howey et al., 2016, 2020), plant distribution (McMichael et al., 2014), and soil and
 148 drought (Palace et al., 2017). MaxEnt has been applied in hydrology to a range of problems
 149 (Singh 1997; Fischer et al., 2020; Westhoff et al., 2014) including to constrain hydrologic model
 150 parameters (Westhoff and Zehe, 2012), map groundwater (Rahmati et al. 2016), evaluate effect
 151 soil structure on hydrologic fluxes via preferential flow paths (Zehe et al., 2010) and characterize
 152 land-surface hydrology (Wang and Bras, 2011; Djebou and Singh, 2015). Importantly, the
 153 MaxEnt model provides valuable information about variable importance with model reliability
 154 that dominates the overall contribution for developing a MaxEnt model. While entropy-based
 155 methods have advantages over traditional statistical methods (Mishra and Coulibaly, 2009),
 156 research regarding the use of entropy theory for understanding snow variability across a
 157 landscape is currently limited (Keum et al., 2018).

158 The main objective of this study is to identify physical drivers controlling spatial
 159 heterogeneity of snow depth focusing on shallow, ephemeral snowpacks using the MaxEnt
 160 framework with information from a UAS-based lidar platform. MaxEnt modeling efforts are
 161 used to evaluate the relative importance of terrain, plant functional type, and soil variables in
 162 identifying the location of the shallowest and deepest snowpack as well as the consistency of
 163 snowpack patterns. This paper is organized as follows. Section 2 provides the study site
 164 information with general land characteristics and weather conditions as well as several field
 165 photos. Section 3 describes the datasets including the UAS lidar snow depth and physical static
 166 variables. The description of the MaxEnt model is included in Section 3.3. Section 4 details the
 167 results of spatial patterns of the lidar snow depth from two flights measured in different winters
 168 and the dominant drivers contributing to the spatial heterogeneity of snow depth. Section 5 offers
 169 a discussion about new findings in the MaxEnt results with respect to previous studies as well as
 170 strengths and limitations of the UAS lidar. Conclusions and future perspectives are drawn in
 171 section 6.

172 2. Study site

173 This study was conducted at the University of New Hampshire Thompson Farm Research
 174 Station in southeast New Hampshire, United States (N 43.10892°, W 70.94853°, 35 m above sea
 175 level), which was chosen for its mixed hardwood forest and open field land covers (Perron et al.
 176 2004; Burakowski et al., 2015; Burakowski et al., 2018; Sanders-DeMott et al. 2020) that are
 177 characteristic of the region (**Figure 1**). Thompson Farm has an area of 0.83 km² and little
 178 topographic relief (18 to 36 m ASL) (Perron et al., 2004). The agricultural fields are actively
 179 managed for pasture grass. The mixed coniferous and deciduous forest is composed primarily of
 180 northern red oak (*Quercus rubra*), white pine (*Pinus strobus*), shagbark hickory (*Carya ovata*),
 181 red maple (*Acer rubrum*), and white oak (*Quercus alba*) (Perron et al., 2004). There are two
 182 “wood roads” that run north-south through the pasture and into the western forest section. The
 183 winter climate at Thompson Farm is characterized by cold, maritime winter climate with a mean
 184 winter air temperature of -3.0°C, snowfall of 114 cm (NH State Climate Office, 2014), and three
 185 weeks to over three months of days with snow cover (Burakowski and Hamilton, 2020). Snow
 186 depth can range from a trace up to 94 cm and typical snow density ranges from 100 to 400 kg/m³
 187 (Burakowski et al. 2013).



188

189 **Figure 1.** Study location with a leaf-off image of Thompson Farm, Durham, New Hampshire,
190 United States (left) with examples of photos showing the field and forest conditions (right) in
191 December 2019 (Snow-on image with flight lines is provided in **Figure S1**).

192 3. Datasets and Methods

193 3.1 UAS lidar snow depth surveys

194 UAS lidar snow depth surveys were conducted at the Thompson Farm Research Station
195 during two consecutive winter seasons. This study compares two lidar derived snow depth
196 products that represent the distribution of snow depth at a spatial resolution of one meter. Snow
197 surface elevations were collected on January 23rd, 2019 (hereafter termed water year [WY] 2019)
198 and December 4th, 2019 (WY2020). The respective bare earth baseline elevations were collected
199 following snowmelt on April 11th, 2019 and March 18th, 2020. The total area surveyed was
200 approximately 0.11 km², of which 0.7 km² was open field and 0.4 km² was mixed deciduous
201 (dormant) and coniferous forest.

202 Snowpacks for both dates were formed by heavy and wet snowfall. Total precipitation
203 from the initial snowfall event to the date when the UAS survey was conducted was 27 mm and
204 45 mm, respectively (January 19th to 23rd, 2019 for WY2019; December 1st to 4th, 2019 for
205 WY2020). For both events, the wind speed during snowfall and prior to the UAS lidar surveys

were minimal, averaging approximately 2.5 m/s (see the windrose diagrams in **Figure S2**).
 Based on a directional semivariogram analysis, there were no clear relationships between the
 wind speed and direction, the parameters of the associated semivariogram, and the deposition
 and redistribution of snow for either event.

A heavy lift quadcopter manufactured by UAV-America was used to carry lightweight
 and inexpensive Lidar and GNSS-inertial sensors. The Lidar sensor used was the Velodyne VLP-
 16. The VLP-16 has 16 independent infrared lasers that rotate 360 degrees along the horizontal
 axis and are evenly spaced from -15 to +15 degrees along the vertical axis. The sensor was
 configured to only collect the strongest return per laser pulse, resulting in approximately 300,000
 laser shots per second. Lidar distance observations were georeferenced using the UAS trajectory
 and attitude observed with the Applanix APX-15 IMU/GPS. The APX-15 uses a high-
 performance GNSS receiver that achieves a positional accuracy of 2-5 cm following post-
 processing. Post-processing was accomplished using the POSPac UAS software package and a
 nearby continuously operating reference station Global Navigation Satellite Systems (GNSS)
 base station. Micro electromechanical systems (MEMS) sensors are also used by the APX-15 to
 capture UAS attitude with uncertainties of 0.025-degree roll and pitch, and 0.08-degree true
 heading. The APX-15 collects positional and attitude observations at a rate of 200 Hz, enabling
 the high-frequency Lidar observations to be accurately georeferenced. UAS flights were
 conducted at an altitude of 81 meters. This altitude was selected to achieve maximum swath
 width (~150m) while remaining in the operational range limits of the VLP-16 Lidar sensor. A
 lawn mower flight plan with a targeted swath overlap of 40% was used on the WY2019 survey
 and the respective baseline. In an effort to achieve a denser point cloud, a crossed flight plan
 with a sensor swath overlap of 40% between parallel flight lines was used for the WY2020
 survey and the respective baseline (**Figure 1**). Similar point densities were achieved between the
 two flights. A flight speed of 7 m/s was used for both flights. Point Clouds were filtered to
 remove all non-ground laser returns using a progressive morphological filter as part of the R
 package LidR. Classified lidar returns were then averaged over a one-meter grid to create digital
 elevation models (DEMs) for the bare earth and snow surfaces. Snow depth maps were
 constructed by simply subtracting the snow-on DEM from the bare-earth DEM.

In our previous study which validated the lidar snow depth with in situ magnaprobe snow
 depth measurements, the lidar snow depth measurements had mean absolute differences (MAD)

237 and root mean squared difference (RMSD) values of 0.96 cm and 1.22 cm, respectively, in the
 238 open field, and the MAD and RMSD values were 9.6 cm and 10.5 cm, respectively, in the forest
 239 in WY2019 (Jacobs et al., 2021). Due to the relatively large differences in the forest, an
 240 independent study was conducted to compare difference in snow depth measurements between
 241 the magnaprobe and a Federal snow tube sampler. The magnaprobe consistently overestimated
 242 snow depth measurements as compared to the Federal sampler likely due to smaller diameter of
 243 the magnaprobe instrument (magnaprobe: 1.27 cm vs. Federal sampler: 4.13 cm) that was able to
 244 penetrate the unfrozen soil and leaf litter under the snow. The lidar snow depth map in WY2020
 245 had MAD and RMSD of 1.6 cm and 2.0 cm, respectively, in the open field and MAD and RMSD
 246 of 3.0 cm and 3.9 cm, respectively, in the forest under conditions of frozen soils. The improved
 247 agreement between the magnaprobe and the lidar for the second campaign likely reflects the
 248 frozen forest soils and is a better indicator of typical lidar performance in the forest. For this
 249 study, we consider the lidar measurements to provide reliable measures of snow depth variations
 250 across the study area as needed to characterize the spatial variability of ephemeral, shallow
 251 snowpack structure.

252 3.2 Physical variables

253 Topographic and soil variables were investigated as potential physical drivers of field
 254 scale snow depth spatial heterogeneity. Variables included in this study were inter-pixel standard
 255 deviation of lidar returns (STD), aspect, slope, roughness, topographic compound index (TCI),
 256 plant functional type, shadow hours, saturated hydraulic conductivity (K_{sat}), and soil organic
 257 matter (**Figure 2**). Mapped at a one-meter scale, all physical variables are derived from our UAS
 258 observations except the two soil variables. The soil variables, saturated hydraulic conductivity
 259 and organic matter of the soil at depth of 0–5 cm were obtained from Probabilistic Remapping of
 260 SSURGO (POLARIS) soil property maps at 30-m spatial resolution (Chaney et al., 2016; 2019).
 261 To avoid additional errors from a spatial downscaling process, the soil maps were disaggregated
 262 to 1 m² resolution without applying any interpolation techniques.

263 The percent slope and aspect were calculated using Horn's method (Horn, 1981). Surface
 264 roughness was calculated as the largest intra-cell difference of a central pixel and its eight
 265 surrounding cells. STD is the standard deviation of the lidar returns within each pixel and is a
 266 measure of the small-scale surface roughness. Topographic compound index (TCI), also known

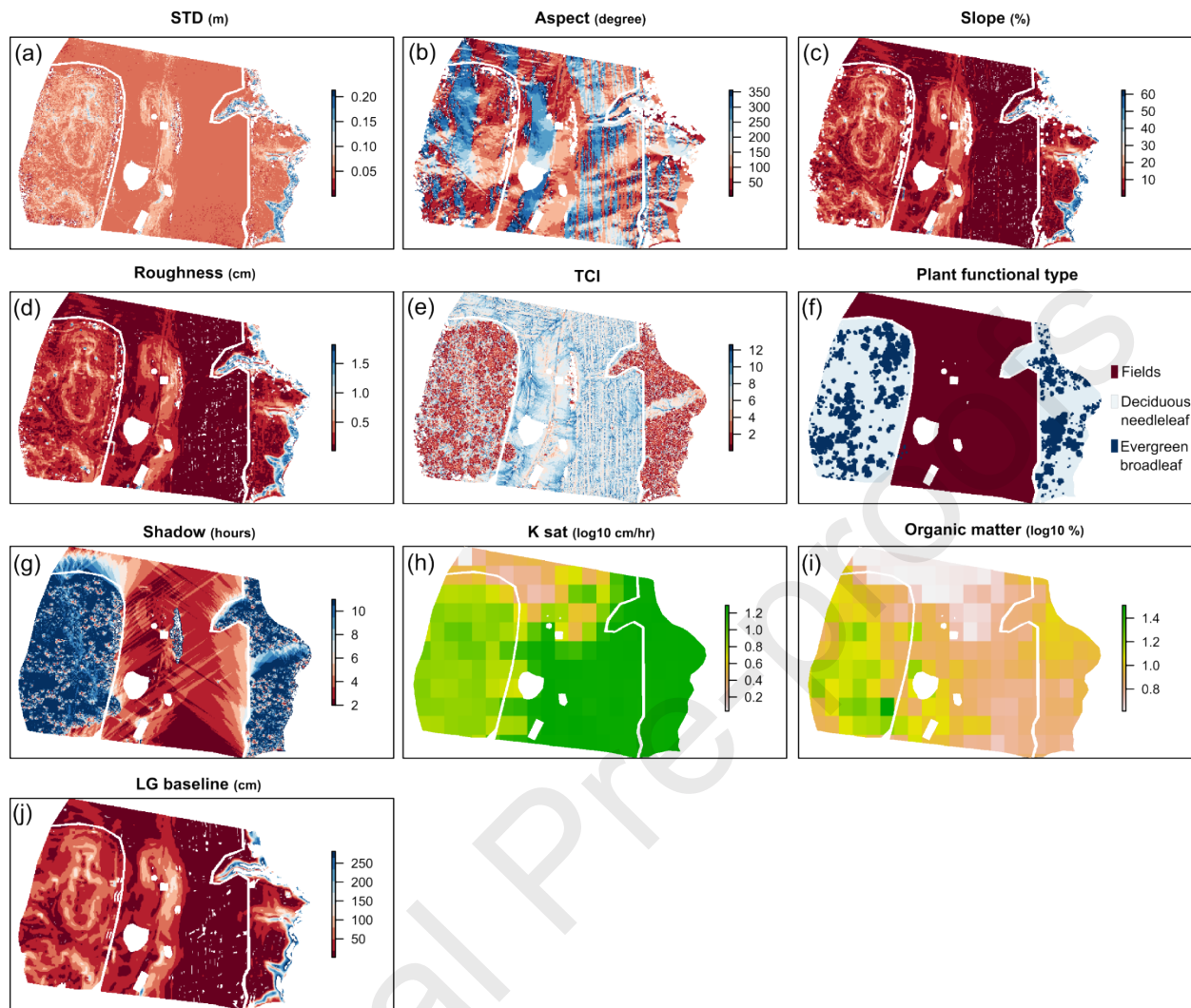
267 as or topographic wetness index, is used to estimate the surface water that might accumulate
 268 across a landscape (Sørensen et al., 2006; Howey et al., 2016). This metric is computed as
 269 $A/\tan B$, the cumulative upslope region (A) that drains through a specific point along a contour
 270 path (B). Total shading hours represents the number of hours from 7 am to 5 pm that a pixel was
 271 in the shade on the survey date and was calculated using the unfiltered UAS-lidar digital terrain
 272 model (DTM) and the incidence angle of the sun on the survey date. Binary shadow maps
 273 (shadow or no-shadow) were made for each hour from 7 am to 5 pm then merged to count the
 274 number of hours that a pixel was in the shade. To characterize the local variability of snow depth
 275 (~10 m), the local gradient of the snow surfaces and their respective baselines (snow-off) were
 276 calculated using image convolution through a 9 x 9 pixel moving window. The horizontal
 277 gradient within the moving window was calculated as the difference between the mean pixel
 278 values to the left of the center column and the mean pixel values to the right of the center
 279 column. The vertical gradient within the moving window was calculated as the difference
 280 between the mean pixel values above the center row and the mean pixel values below the center
 281 row. The total local gradient (LG) was then calculated by summing the gradient components as
 282 follows:

283

$$284 \quad \text{Total local gradient} = \sqrt{\text{Horizontal gradient}^2 + \text{Vertical gradient}^2} \quad (1)$$

285

286 At least 50% of the pixels within each window had to have snow depth data (e.g.,
 287 percentage of pixels with data to the left of the center column). If this condition was not met for
 288 any portion of the window used to calculate the gradient components, a value of not available
 289 (NA) was recorded for the total gradient at this location.



290

291 **Figure 2.** Spatial maps of the six topographic variables, (a) inter-pixel standard deviation of lidar
 292 returns (STD), (b) aspect, (c) slope, (d) roughness, (e) topographic compound index (TCI), (f)
 293 plant functional type, and (g) shadow hours, and two soil variables, (h) saturated hydraulic
 294 conductivity (K_{sat}) and (i) organic matter, plus (j) the local gradient (LG) of baseline used as
 295 input variables for the Maximum Entropy model.

296

3.3 Maximum Entropy (MaxEnt) model

297 The concept of MaxEnt originates in information theory (Jaynes, 1957). The principle of
 298 the MaxEnt states that the most appropriate distribution to represent a given data set is the one
 299 with the largest entropy that satisfies the constraints of prior information about the target
 300 distribution (Phillips et al., 2006). The constraints mean that the expected value of each predictor
 301 variable should match its empirical mean value for a set of sample points taken from the
 302 distribution. In spatial modeling, MaxEnt, as a machine learning approach, uses the spatial

303 location of focal features and predictor (input) variables to extrapolate these features across a
 304 landscape where those predictor variables are present (Baldwin, 2009; Phillips et al., 2006).
 305 MaxEnt is theoretically similar to generalized linear models (GLMs) and generalized additive
 306 models (GAMs). For example, if the probability of occurrence is modeled by a GAM using a
 307 logit link function, the model form is the same as the log probability of a pixel in MaxEnt with
 308 threshold features (Phillips et al., 2006). While the Maxent has similarities to existing methods
 309 such as GLM and GAMs for spatial distribution modeling, important differences exist between
 310 the Maxent and GLM/GAMs, leading to different predictions. When the probability of
 311 occurrence is modeled by GLM/GAMs, absence data are required. In many disciplines, survey
 312 techniques, birds for example, or archaeological sites, only presence data are able to be recorded
 313 with certainty. In addition in many regions, survey data are limited in their spatial coverage.
 314 Thus background pixels, instead of true absence data, must be used, and the model output is less
 315 clear cut (Ferrier et al., 2002). In contrast, the Maxent can model a probability distribution over
 316 the pixels in the study area without absence data. In addition, because MaxEnt is a generative
 317 approach, whereas GLM/GAMs are discriminative, it can often give better prediction results
 318 when the amount of training data are relatively small (Ng and Jordan, 2001).

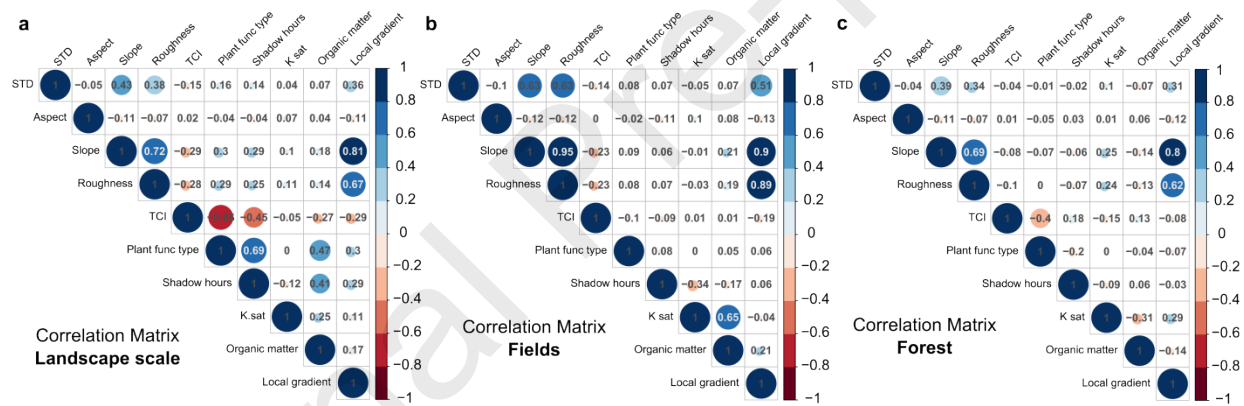
319 While applications of MaxEnt have expanded to various disciplines including a range of
 320 hydrologic problems (Singh 1997; Fischer et al., 2020; Westhoff and Zehe, 2012; Rahmati et
 321 al. 2016; Wang and Bras, 2011), to our knowledge, there have been no studies seeking to
 322 understand snowpack spatial variability using this approach. In this study, we used the MaxEnt
 323 framework to identify physical variables that control the spatial variations of the snow depth
 324 estimated from a UAS lidar system in the context of a shallow, ephemeral snowpack. The
 325 important variables identified from the MaxEnt models are considered as a proxy for physical
 326 drivers to generate spatial heterogeneity of snowpack because they dominantly contribute to
 327 predicting the deep or shallow snow depths. There are two types of variable importance values
 328 from the MaxEnt model, percent contribution and permutation importance. The MaxEnt model
 329 keeps track of which input variables are contributing to fitting the model while it is being trained.
 330 In the training process, each step increases the gain of the model by modifying the coefficient for
 331 a single variable. The percent contribution is obtained by converting the gains to percentages at
 332 the end of the process. The permutation importance is defined as the decrease in a model score
 333 when a single feature value is randomly shuffled. This procedure breaks the relationship between

334 the input variables and the dependent variable, thus the drop in the model score is indicative of
335 how much the model depends on the feature. This importance for each input variable is
336 determined by randomly permutatiing the values of the variable among the training points (See
337 details in Phillips, 2006). Percent contribution results are presented in the body of the paper, and
338 permutation importance results are included in the Supporting Information.

339 To check the reliability of the MaxEnt models, the area under the receiver-operator curve
340 (AUC) is used in this study, which indicates the predictive capacity of the model (Merow et al.,
341 2013). AUC indicates the probability that a randomly chosen presence point is ranked higher
342 than a randomly chosen absence point (0 to 1). An AUC value of 0.5 is the same as a random
343 guess of presence/absence. The closer an AUC value is to 1, the more reliable the predictions
344 from the MaxEnt model. A model with an AUC over 0.75 is often considered to accurately
345 estimate sample data (Phillip and Dudík, 2008).

346 **4. Results**347 **4.1 Relationship among physical variables**

348 Before conducting the MaxEnt model analysis to identify physical drivers controlling
 349 spatial variability of snow depth, cross-correlation matrices among the physical input variables
 350 were calculated for (1) landscape scale (i.e. fields and forest combined), (2) fields, and (3) forest.
 351 **Figure 3** shows the cross-correlation matrices with the Pearson correlation coefficients (R-values)
 352 with different colors. For all three areas, roughness is strongly correlated with slope ($R = 0.69$,
 353 0.95, and 0.69 for landscape scale, fields, and forest, respectively). While slope and roughness
 354 are moderately correlated with the standard deviation of lidar returns (STD; $R = 0.63$ for both) in
 355 fields, they are less strongly correlated ($R = 0.39$ and 0.34) in forest areas. For the fields, there is
 356 also a strong correlation ($R = 0.65$) between saturated hydraulic conductivity (K_{sat}) and organic
 357 matter of soils.



358

359 **Figure 3.** Cross-correlation matrices for (a) landscape scale (forest and fields combined), (b) fields, and (c)
 360 forest based on the boundaries from Figure 1.

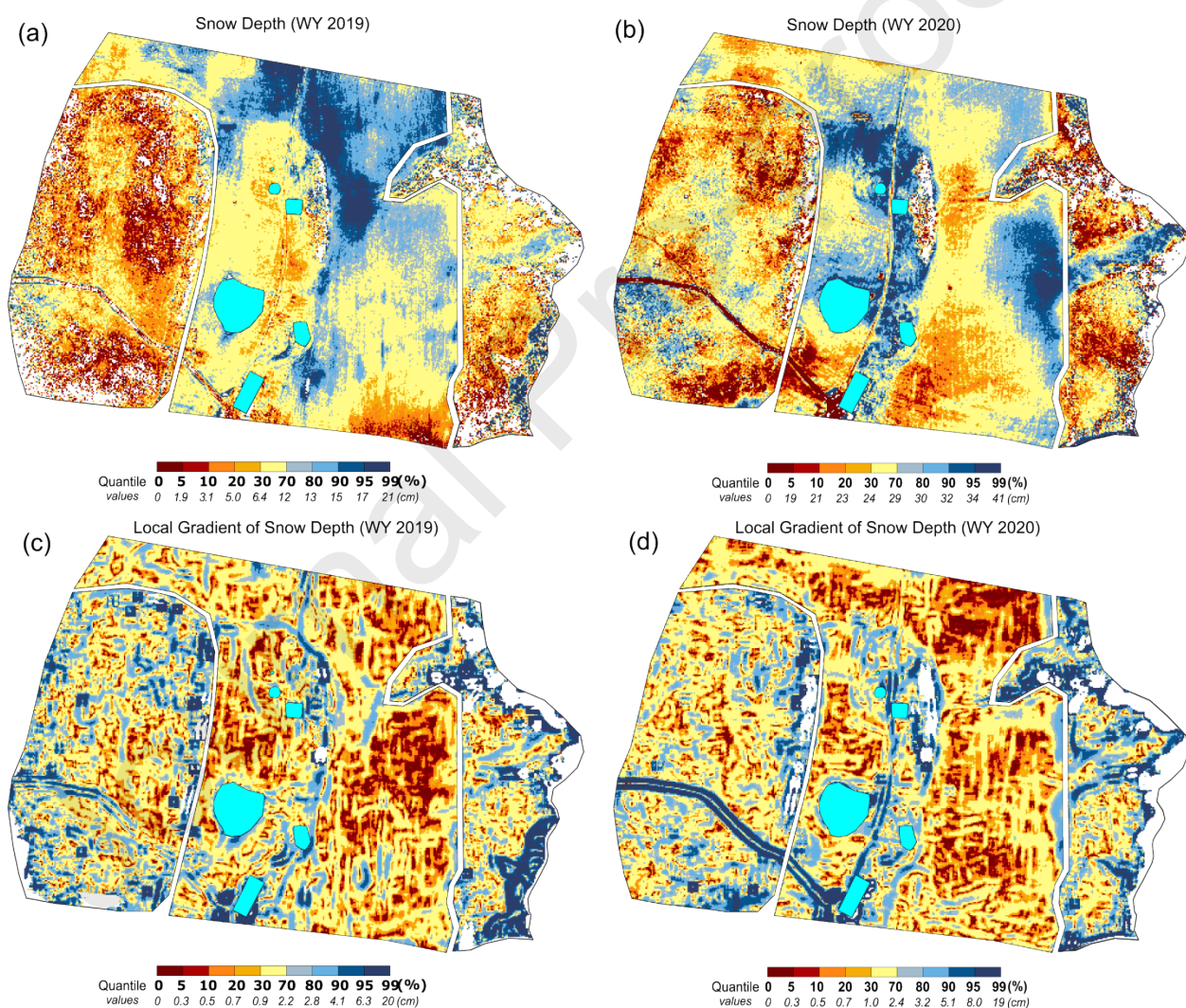
361 **4.2 Spatial patterns of snow depth**

362 The UAS lidar-based snow depths, mapped by subtracting snow-off DTMs from snow-on
 363 DTMs, reveal a shallow snow depth ranging from less than 2 cm to over 21 cm in WY2019
 364 (mean = 9.4 cm; standard deviation = 9.7 cm) and up to 41 cm in WY2020 (mean = 26.9 cm;
 365 standard deviation = 15.2 cm) (**Figure 4** and **Table 1**).

366 The shallower snow depths (lower 30%) were 6.4 cm and 24 cm and deeper snow depths
 367 (higher than 70% for each map) were 12 cm and 29 cm in WY2019 and WY2020, respectively.
 368 Despite having different magnitudes of snow depth between the two dates, there were similar

369 spatial patterns. Deeper snow depth values (blue) existed in the fields and shallower snow depths
 370 (red) in forest (**Figure 4**). Compared to the forest snowpack, the field snow depth had relatively
 371 high spatial variability and less coherent patterns. In the field, the deeper snow is in the northeast
 372 areas in WY2019. However, in WY2020, the deeper snow occurred in the middle and east areas.
 373 A shallow and spatially consistent snowpack occurred in forest areas. In the deciduous forest
 374 type, the snow depth was consistently higher than that in coniferous forest, especially in the east
 375 forest (see the plant functional type map in **Figure 2f**). The shallowest snowpack was found in
 376 coniferous forest type.

377



378

379

380 **Figure 4.** 1-m gridded unpiloted aerial system (UAS) Lidar-based snow depth maps (a and b)
 381 and their local gradient maps (c and d) in WY2019 (left) and WY2020 (right side). To emphasize
 382 the spatial distribution of shallower (lower) or deeper (higher) values of snow depth (local

383 gradient), the color bars are divided by quantile values (0, 5, 10, 20, 30, 70, 80, 90, 95, and 99%)
 384 for each map. The cyan color areas indicate masked area s(e.g. buildings and ponds).

385
 386 Likewise, spatially coherent patterns of the local gradients of snow depth are readily
 387 discernible between the two UAS surveys (**Figure 4c and d**). Lower local gradient values (red),
 388 indicating a relatively consistent snow depth, existed in the east fields. Higher gradients (blue)
 389 were found in the field to forest transitions and roads. In the forest areas, the lower local
 390 gradients generally appeared in coniferous forest. High local gradients are consistently found at
 391 the forest edge.

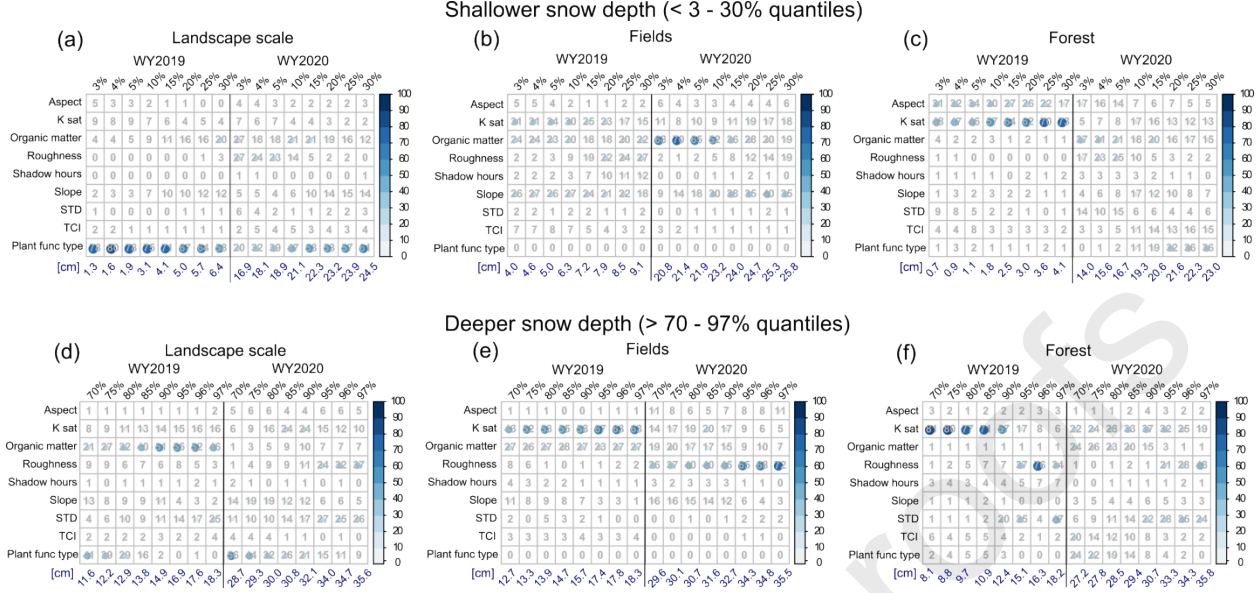
392 **Table 1.** Summary of snow depth and local gradient of snow depth in January (WY2019) and
 393 December 2019 (WY2020)

Areas	Snow depth (cm)						Local gradient of snow depth (cm)					
	WY2019			WY2020			WY2019			WY2020		
	Mean	Std	99%	Mean	Std	99%	Mean	Std	99%	Mean	Std	99%
Landscape	9.4	9.7	21.7	26.9	15.2	40.9	2.7	10.8	19.8	2.7	6.7	19.3
Fields	11	3.8	19.9	27.8	6.8	38.2	1.6	4.1	8.1	2	5.4	14.1
Forest	7.2	13.8	27.4	25.8	21.1	46.8	3.9	15.3	35	3.6	7.8	21.5

394

395 4.3 Physical drivers contributing spatial variability of snow depth

396 To determine the most relevant physical drivers that contribute to the spatial
 397 heterogeneity of snow depth, the relative importance of the input variables from the MaxEnt
 398 model with different thresholds was quantified. **Figure 5** shows the relative contribution of the
 399 nine input variables from each MaxEnt run using the shallow and deep snow depth values within
 400 thresholds. Larger percentages indicate those variables that play a greater role in predicting the
 401 suitability of shallower or deeper snow depth.



402

403 **Figure 5.** Variable importance from the MaxEnt models for shallower and deeper snow depth observed in
 404 WY2019 (left) and WY2020 (right side of each subfigure). Shallower or deeper snow depth is
 405 determined by thresholds. Shallower snow depth is defined as less than 3% (extremely shallow) to 30%
 406 quantiles (moderately shallow) of the entire snow depth values for the three areas: (a) landscape (forest
 407 and fields combined), (b) fields, and (c) forest, respectively. Deeper snow depth values are from larger
 408 than 97% (extremely deep) to 70% quantiles (moderately deep) for the three areas: (d) landscape, (e)
 409 fields, and (f) forest, respectively. Permutation importance values for the snow depth are also provided in
 410 Supporting information (**Figure S3**).

411 For shallow snow depths (top panels; **Figure 5a - c**), plant functional type is the most
 412 important variable in the landscape scale, especially in the WY2019 snow depths, which were
 413 shallower than the snow depths from WY2020. For the snow depths in WY2020, soil organic
 414 matter and roughness contribute somewhat (e.g., both are 27% for the lowest 3% quantile of
 415 snow depth). In the fields, soil variables, organic matter and K_{sat}, and slope are generally
 416 important. The contribution of soil organic matter to the shallow snow depths in WY2020 is very
 417 strong, ranging up to 70%. In the forest, it seems that different variables influence the shallow
 418 snowpack for the two study snowpacks. While K_{sat} and aspect are clearly important to identify
 419 shallow snow depth in WY2019 as compared to other variables, there are no dominant variables
 420 in WY2020. Soil organic matter (21% to 37%) and roughness (17% to 23%) are somewhat
 421 important for extremely shallow snow depths (less than 3% to 5% quantiles).

422 For deep snow depths (bottom panels; **Figure 5d - f**), different variables contribute to
 423 snow depth for the two study snowpacks. While the organic matter is the dominant control in
 424 WY2019, landscape scale, roughness and STD are more important in WY2020. In the fields, K_{sat}

425 and organic matter indicate locations of deep snow in WY2019, but roughness is the most
 426 important variable in WY2020. In the forest, the variable contributions differ by snowpack. For
 427 the deepest snow depth (95% to 97% quantiles), roughness (and STD) is important but the
 428 contributions of K_{sat} and organic matter gradually increase when the threshold for deep snow is
 429 decreased.

430 In summary, plant functional type is an important explanatory variable for mixed
 431 vegetation areas, especially in predicting the shallow snow depth. Soil variables, organic matter
 432 and K_{sat} , contribute to both shallow and deep snowpacks. Roughness and STD are also important
 433 particularly for the snow depth in WY2020 rather than in WY2019. Contrary to expectations,
 434 shadow hours, aspect, and TCI had limited ability to identify the relatively shallow or deep snow
 435 depth in the MaxEnt framework.

436 Predicted suitability maps of shallower or deeper snow depth can be estimated from the
 437 MaxEnt models developed for target ranges. Based on the training points with input variables,
 438 the MaxEnt model provides suitable locations with likelihood where the range of snow depth
 439 likely exists. For example, **Figure 6** includes predicted suitability maps for the locations where
 440 the snow depth is less than the 5% quantile and greater than the 95% snow depth quantile for the
 441 two snowpacks. These maps are the combination of the two maps developed by the MaxEnt
 442 models for fields and forest, respectively. In WY2019 (**Figure 6a**), locations with high predicted
 443 suitability (dark red) for shallow snowpack correspond to locations with shallow snow depth
 444 (e.g., west forest, south fields, and central fields near ponds; see **Figure 4**). In WY2020 (**Figure**
 445 **6b**), distributions with high suitability also agreed fairly well with the shallow values from the
 446 snow depth map (e.g., southwest fields and east forest). For the 95% snow depth quantile,
 447 predicted maps with high suitability values captured areas where deep snow depth exists (**Figure**
 448 **6c and d**; e.g., northeast fields in WY2019, central fields near the small buildings in WY2020,
 449 and east forest in both months).

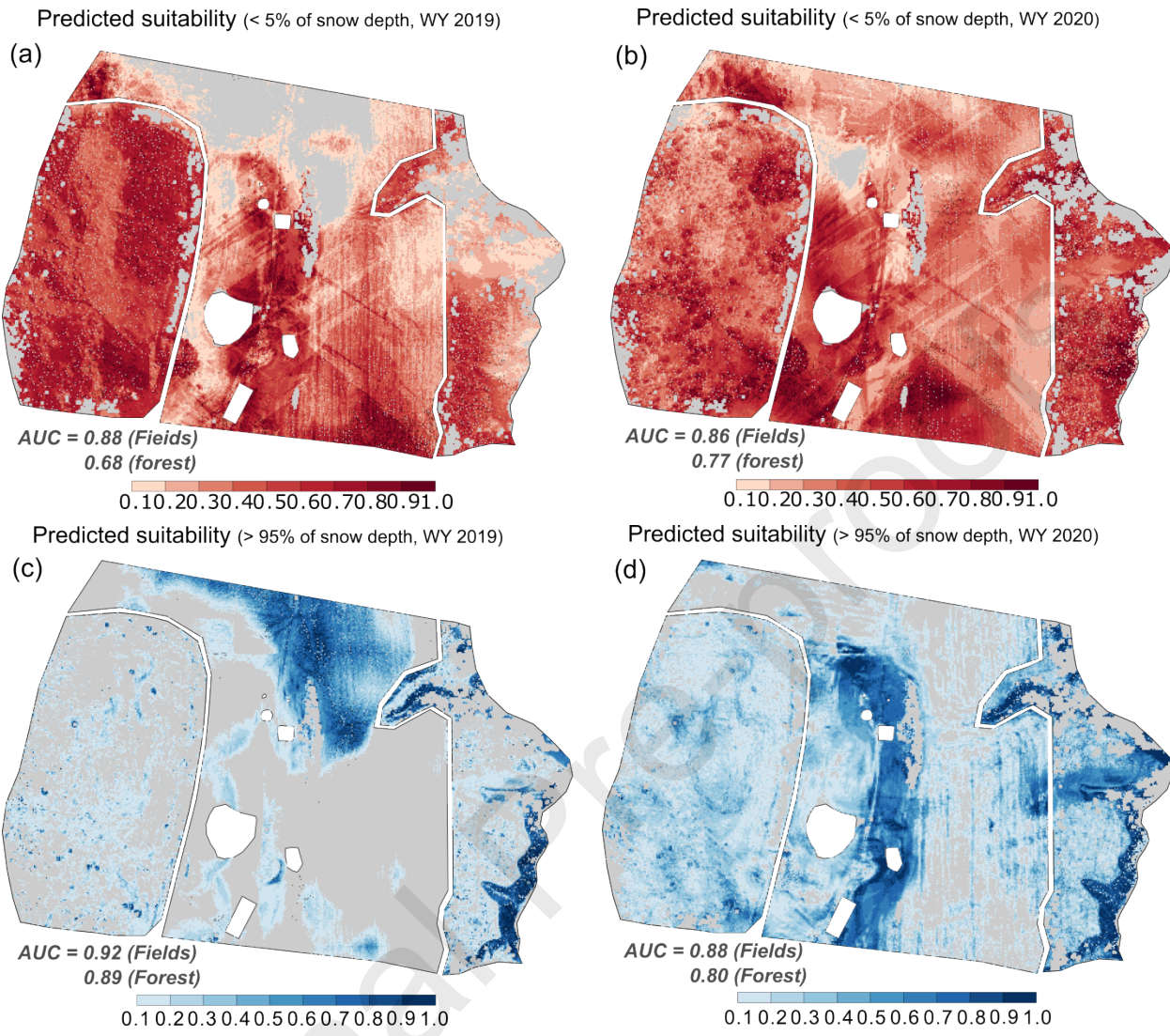
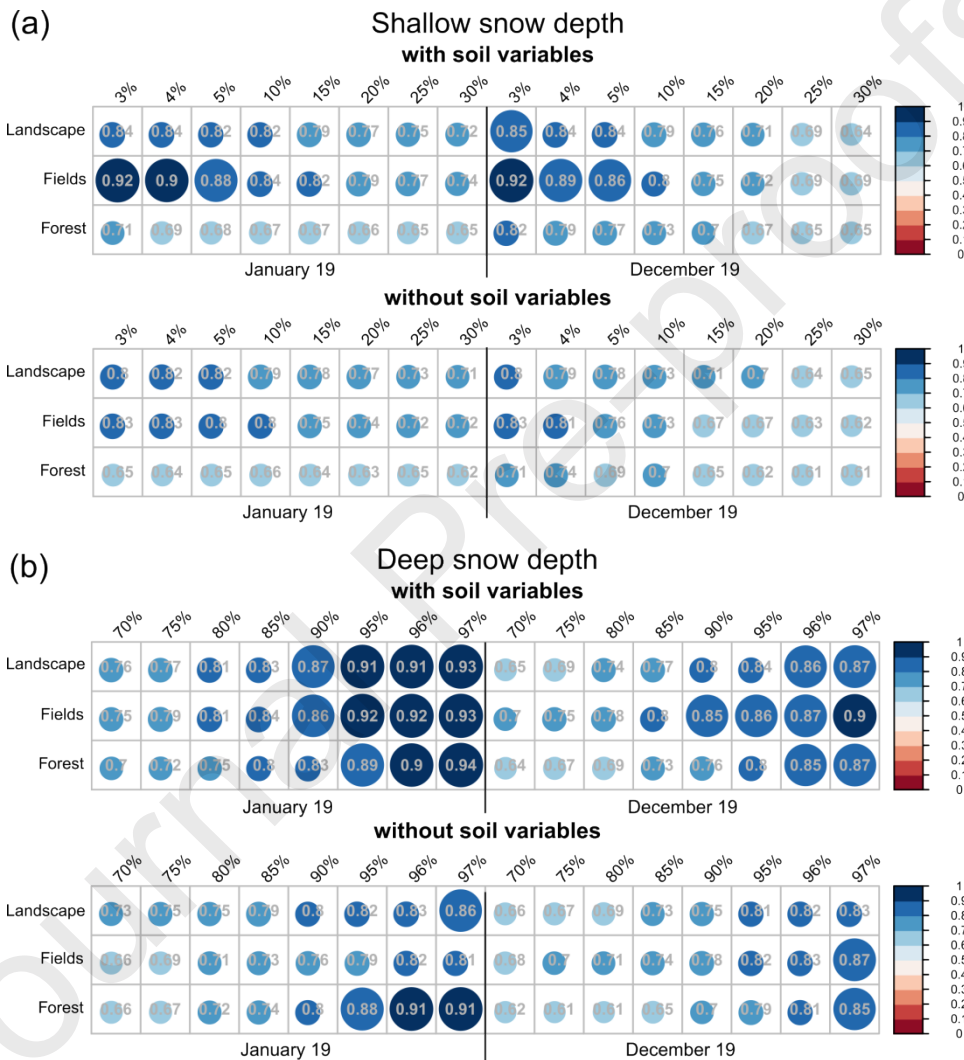


Figure 6. Predicted suitability maps of shallower (< 5 % quantile; a and b) and deeper (> 95 % quantile; c and d) snow depth from the Maximum Entropy (MaxEnt) models in WY2019 (left) and WY2020 (right side), separately. The predicted suitability ranges 0 (no possibility) to 1 (100% possibility exists for the range of snow depth). The area under the receiver-operator curve (AUC) indicates the predictive capacity of the model. Generally, a model with an AUC over 0.75 is often considered to accurately predict target data (Phillip and Dudík, 2008).

In an effort to better discern the effect of soil variables such as K_{sat} and organic matter on the reliability of the MaxEnt model, AUC values are compared for models that include and exclude the two soil variables (**Figure 7**). The AUC values from the MaxEnt models for the shallowest (3% to 5%) and deepest snow depths (95 to 97% quantiles) are higher than the moderate snow depths (10% to 30% and 70% to 95%). For both shallow and deep snow depths, the MaxEnt models with soil variables have higher AUC values than the MaxEnt models without

465 soil variables. This tendency is more apparent in the field than the forest. For fields with shallow
 466 snow depth (**Figure 7a**), AUC values with soil variables range from 0.86 to 0.92 for the 3% to 5%
 467 snow depth quantiles, while the values without soil variables range from 0.76 to 0.83. For fields
 468 with a deep snowpack (**Figure 7b**), there is a more modest influence. The AUC values with soil
 469 variables for the 95% to 97% quantiles range from 0.86 to 0.93, while the values without soil
 470 variables are range from 0.79 to 0.87.

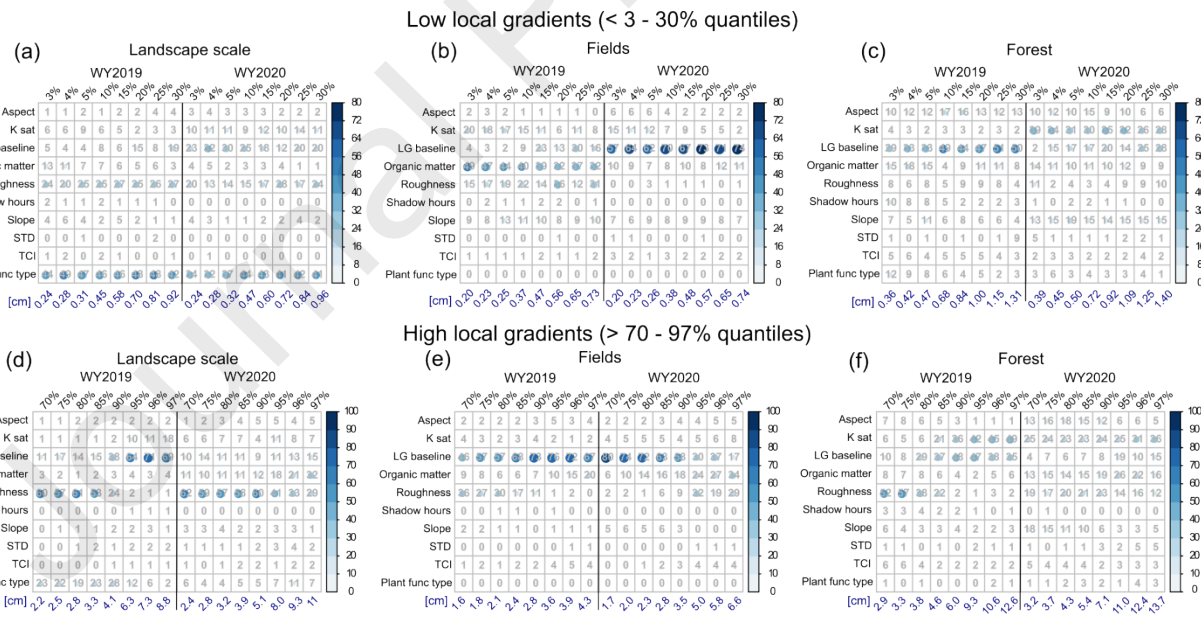


471
 472 **Figure 7.** Comparison of the Area Under the receiver-operator Curve (AUC) values of the MaxEnt
 473 models (a) with and (b) without soil variables (organic matter and saturated hydraulic conductivity) for
 474 shallow and deep snow depths observed in WY2019 and WY2020.

475 4.4 Localized variability of snow depth

476 The relative contributions of the static variables on the snow depth local gradients were
 477 computed in the MaxEnt framework for locations having lower (less than 3% to 30%) and higher

478 local gradients (greater than 7% to 97%) (**Figure 8**). For this analysis, the static variable
 479 included the nine input variables previously used as well as the local gradient mapped during the
 480 baseline (snow-off) flight. Variables with larger percentages indicate that the input variables play
 481 a greater role in predicting the local gradients and typically improving the MaxEnt's reliability.
 482 For low local gradients of snow depth, implying locally homogeneous snowpack conditions
 483 within 10 m (top panels), plant functional type was the most important variable (32% – 49%) for
 484 landscape scale, especially in the shallower snow depth map from WY2019 (**Figure 8a**).
 485 Roughness and the baseline local gradient were of secondary importance in WY2019 and
 486 WY2020, respectively. Roughness contributed 24% and baseline local gradient contributed 23%
 487 for the less than 3% quantile of local gradients. In the fields, there were clear differences in
 488 important variables between the two snowpacks (**Figure 8b**). While soil variables, organic
 489 matter and K_{sat} , and roughness were important for WY2019, the baseline's local gradient was the
 490 strongest contributor for WY2020. In the forest, there were no dominant variables, except for the
 491 baseline's local gradient for WY2019 (**Figure 8c**). Aspect, shadow hours, STD, and TCI did not
 492 play a role in the location of low local gradients for the overall site, nor for the field and forest
 493 areas.



494
 495 **Figure 8.** Variable importance from the MaxEnt models for low (top) and high (bottom panel) local
 496 gradients of snow depth observed in WY2019 (left) and WY2020 (right side of each subfigure). Low or
 497 high local gradients of snow depth are determined by thresholds. Low local gradient is defined as less
 498 than 3% (extremely low) to 30% quantiles (moderately low) of the entire local gradient values for the
 499 three areas: landscape (forest and fields combined), fields, and forest, respectively. High local gradient

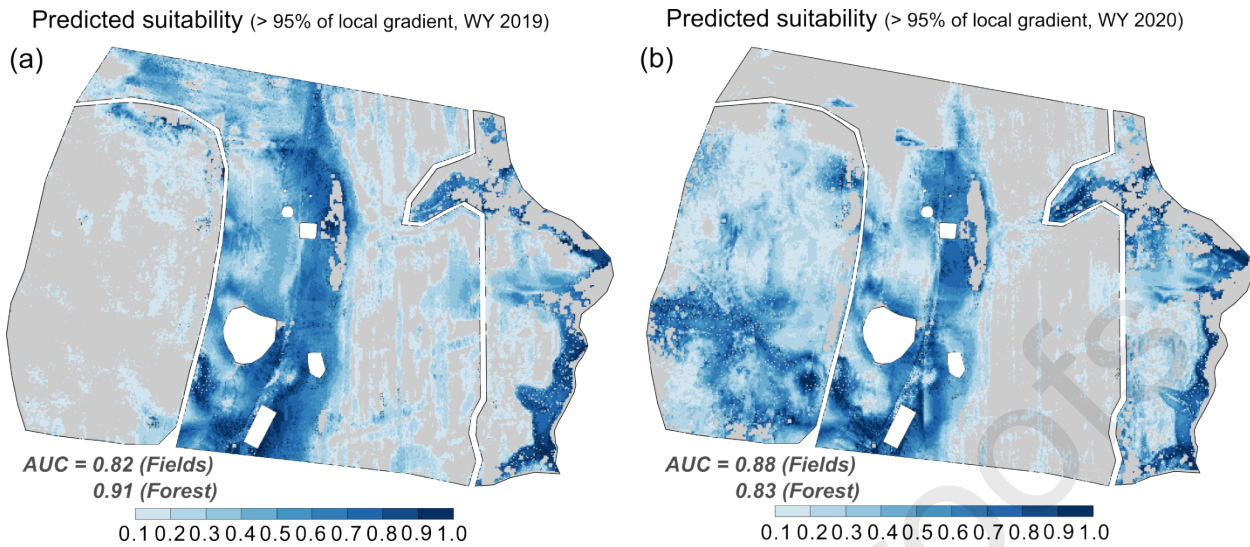
500 values are from larger than 97% (extremely high) to 70% quantiles (moderately high). Permutation
 501 importance for the local gradients are also provided in Supporting information (**Figure S4**).

502 For high local gradients of snow depth (bottom panels of Figure 8), roughness and the
 503 baseline local gradient are important for identifying landscape scale transitions. For the WY2019
 504 snowpack, the contributing percentage of the baseline's local gradient was around 70% for the
 505 extremely high local gradients (95% to 97% quantiles). The contribution of the baseline local
 506 gradient decreased with decreasing thresholds, and roughness's contribution increased indicating
 507 a transition between the two highly correlated variables (**Figure 8d**). In fields, the baseline local
 508 gradient was the dominant control and contributed up to 80% (**Figure 8e**). Organic matter was
 509 also somewhat important (up to 20% to 34%) for the highest local gradient of snow depth (higher
 510 than 95% quantiles). In the forest, while there were no dominant variables as compared to fields
 511 or landscape scale, for WY2019, K_{sat} and baseline's local gradient were important (49% and
 512 36%, respectively; **Figure 8f**). The contribution of roughness gradually increases with
 513 decreasing the quantiles (particularly from 70% to 85% quantiles).

514 In summary, plant functional type is valuable for predicting the low local gradients of the
 515 snowpack at the landscape scale. Within a single plant functional type, the baseline's local
 516 gradient and roughness control the locations of both the low and high local gradients of snow
 517 depth. Soil variables also contribute modestly to identifying spatial variability in the localized
 518 snowpack. Contrary to our expectations, shadow hours, aspect, and TCI had marginal
 519 contributions for localized snowpack variations at the 10 m scale using the MaxEnt framework.

520 In contrast with predicted suitability maps of snow depth, the two predicted suitability
 521 maps of high local gradients have relatively similar spatial patterns for the two snowpacks,
 522 except for the west forest (**Figure 9**). Because the baseline's local gradient and roughness were
 523 the dominant controls needed to predict the local gradients of snowpack, the spatial distributions
 524 of baseline's local gradient and roughness are reflected in the predicted maps (compare to the
 525 input variable maps in **Figure 2**).

526



527

528 **Figure 9.** Predicted suitability maps of the high local gradient of snow depth maps ($> 95\%$ quantile) from
 529 the Maximum Entropy (MaxEnt) models for WY2019 (a) and WY2020 (b).

530 5. Discussion

531 5.1 Physical drivers: Comparison with previous findings

532 Static features such as topography and vegetation rather than local meteorology and
 533 precipitation patterns typically control snow distribution at the local scale. There are numerous
 534 studies, which attempt to characterize spatial snow structures and to identify physical
 535 characteristics affecting the spatial characteristics of the snowpack. Blöschl and Kirnbauer (1992)
 536 investigated the relationship between spatial snow patterns and terrain attributes (e.g., elevation
 537 and slope) in the Austrian Alps. They found no dominant relationship to terrain parameters with
 538 spatial snow depth. Lapen and Martz (1996) found that spatial structures of snow depth are
 539 related to sheltering by topographic obstacles, indicating that drifting is a critical process in the
 540 prairie environment. Mott et al. (2011) mentioned that the driving force for the drifting processes
 541 is the air flow near the surface layer, which is partially shaped by the local terrain. Our results
 542 have similar findings in that there were clear differences in snow depth within the fields (e.g.,
 543 east versus west fields) and transitional areas between fields and forest. Currier and Lundquist
 544 (2018) also found large differences in snow depth for the forest-edge classifications in the
 545 western United States.

546 Soil properties are considered to be a potential feature that can affect spatial variability of
 547 snowpack, yet few studies have investigated how important soil properties are to inform the

548 spatial structure of snow depth as compared to other terrain characteristics. Shook et al. (1993)
 549 investigated area-frequency relationships of snow and soil patches at different stages during the
 550 melting season in prairie and alpine environments. They found that snow and soil patches are
 551 fractals, and their size distribution is predictable, implying that soil properties may potentially
 552 influence such behavior. Redding and Devito (2011) showed differences in the timing of snow
 553 disappearance between two sites with different soil types. They found that mean snowmelt rates
 554 at sites with sand soils were quicker than those at sites with loam soils. However, they could not
 555 conduct significance tests due to the limited measurements from the loam soils. Our findings
 556 suggest that soil properties, organic matter and hydraulic conductivity, can be more important
 557 than shadow hours, aspect, STD, and for modeling the spatial distribution of snow depth, which
 558 is probably because soil properties, especially soil organic matter, impact soil thermal
 559 conductivity (Abu-Hamdeh and Reeder, 2000). The thermal conductivity of soil is highly
 560 dependent on soil density, mineral type, grain size, and moisture content (Farouki, 1981; Penner,
 561 1970; Parikh et al., 1979). In frozen soils, the thermal conductivity is more sensitive to soil type
 562 than non-frozen soils, because the thermal conductivity of ice is more than four times larger than
 563 that of liquid water (Penner, 1970).

564 Recently, Zhu et al. (2019) found that soil organic matter was a dominant factor
 565 controlling the variability of thermal diffusivity at 200 field sites in the high latitude regions. Our
 566 results suggest that spatial differences in soil properties may lead to a spatial discrepancy in heat
 567 transfer between snowpack and soil surface resulting in an enhanced spatial variability of snow
 568 depth even at local scales. With large spatial variability of soil temperature (e.g., less than 10 m
 569 spatial correlation in fields; Mohanty et al., 1995) and frequent patchy snow in shallow
 570 ephemeral snowpacks, the differences in the energy transfer between snow and soil surface
 571 across areas with different snow depths may lead to a heterogeneous spatial distribution of
 572 surface temperatures. Future research with supporting data representing the energy transfer is
 573 needed to address the role of soil properties in the spatial heterogeneity of snowpack.

574 **5.2 MaxEnt framework compared to traditional analysis**

575 To our knowledge, this study is the first to use the MaxEnt model to understand snow
 576 distribution measured using a UAS-based lidar. In the natural science community, the MaxEnt
 577 model is one of the most popular methods for species distribution and ecological modeling (Elith

578 et al., 2006; Merow et al., 2013). The MaxEnt framework provides accurate information about
 579 the degree of importance among the input variables that dominate the overall contribution to
 580 develop the MaxEnt model with model reliability. For the snow science and hydrology
 581 community, this approach can create novel opportunities to identify dominant physical variables
 582 and to advance snow and land surface models by leveraging remotely sensed snow observations
 583 at multiple scales.

584 As a traditional method, variogram approaches including fractal analysis have been
 585 widely used to understand the spatial scaling patterns of snow depth (or SWE) based on the
 586 self-similarity of properties over multiple scales. Deems et al. (2006) conducted a variogram
 587 analysis of snow depth, topography, and vegetation topography datasets from three 1-km² study
 588 areas using an airborne-based lidar system. They found the existence of two different scale areas
 589 from the vegetation topography and snow depth data, separated by a scale break that ranges
 590 between 31 - 56 m for vegetation topography and between 15 - 40 m for snow depth. Trujillo et
 591 al. (2007) also attempted to determine whether the spatial distribution of snow depth has scale
 592 invariance with the interaction with physical features including vegetation, topography, and
 593 winds. They found that a scale break of snow depth was controlled by the scaling characteristics
 594 of vegetation height when wind redistribution of snow was minimal and canopy interception was
 595 dominant. Using fractal analysis, Schirmer and Lehning (2011) investigated seasonal and spatial
 596 changes in the scaling behavior of snow depth. They found that the scale break gradually
 597 increases throughout the snow accumulation season indicating that roughness of the terrain
 598 surface buried by snow may control the scaling behavior.

599 Even though the variogram-type analyses have provided explicit information to
 600 characterize the spatial structure of snowpack, limited information is available to determine the
 601 relative importance among various physical characteristics related to the formation of the spatial
 602 structure of snow depth. Deems et al. (2006) speculated that the length of the scale break might
 603 be due to the terrain relief, and that the physical process change found by the breaks in the
 604 variograms of the vegetation topography potentially influences the scaling patterns of snow
 605 depth. In Trujillo et al. (2007)'s results, none of the breaks in the slope of the log-log plots
 606 between snow depth and the corresponding fields of topography and vegetation topography were
 607 present, while the break in the scaling behavior was controlled by the vegetation characteristics
 608 (e.g. canopy height, canopy-covered area, and distances between trees). Thus, it is expected that

609 the MaxEnt framework with spatially distributed snowpack data supplements the existing
 610 approaches by providing various information about dominant predictor variables along with
 611 spatially predicted suitability maps.

612 In the context of a statistical approach to identify dominant features, a brief discussion
 613 about differences between the MaxEnt and existing popular methods such as the principal
 614 component analysis (PCA) is warranted. The PCA is a widely used approach for reducing the
 615 dimensionality of exploratory data sets to compute the PCs and interpret them from the original
 616 data sets. Particularly, this method is useful when the variables within the data set are highly
 617 correlated. However, the PCs are the linear combination of the original variables which may not
 618 be as readable and interpretable as the original features. Because snowpack responses to
 619 meteorological and land characteristics tend to be complex and, sometimes, have nonlinear
 620 behaviors (Anderton, 2000; Anderton et al., 2004), a PCA might not be successful in addressing
 621 the features. Also, the ordinary PCA method is not suitable to handle categorical variables
 622 because it is hard to find a suitable way to represent distances between variable categories and
 623 individuals in the factorial space. MaxEnt offers several advantages regarding these limitations.
 624 MaxEnt can utilize both continuous and categorical data sets and incorporate interactions
 625 between different variables. It can also provide individual contributions of correlated explanatory
 626 variables on the response variable, allowing each variable to be interpreted separately.

627 **5.3 UAS lidar snow depth sampling**

628 UAS-based lidar has been recently utilized for snow depth mapping (Harder et al., 2020;
 629 Jacobs et al., 2021) providing an opportunity to eliminate many of the drawbacks that arise from
 630 Airborne laser scanning (ALS) and Terrestrial laser scanning (TLS) systems (Deems et al., 2013;
 631 Fey et al., 2019; Hojatimalekshah et al., 2020; Prokop, 2008). Obscuration from clouds found in
 632 ALS systems will rarely be an issue because UAS lidar surveys are generally conducted at an
 633 altitude below 120 meters. Although spatial coverage is typically greatly reduced in UAS
 634 missions relative to other ALS platforms (Harpold et al., 2014; Kirchner et al., 2014), the aerial
 635 perspective and the large sensor swath overlap facilitated by appropriate mission planning and
 636 post-processing provides reduced uncertainties in elevation from those that can result from high
 637 off-nadir viewing angles and occlusion in other ALS platforms. In the same vein, flight
 638 parameters can be readily adjusted to achieve equally dense point clouds over open and forested

639 areas, improving ground finding and resulting in better characterization of vegetation and terrain
 640 mapping. For this study, flight speeds were held constant over both fields and forests, which
 641 produced lower return density over the forested part of our study site. There is some evidence
 642 that vegetation reduces return density due to scattering and absorption (Liu et al., 2020; Jacobs et
 643 al., 2021), so reduced flight speeds over vegetation to account for the reduction in returns could
 644 improve terrain characterization in these settings.

645 **5.4 Limitations**

646 While this study employed a well-validated machine learning approach in a novel setting,
 647 identifying the primary terrain predictors of fine-scale distribution of snow depth, there are
 648 potential limitations to providing generalizable information due to limited experiments and data
 649 availability. The dominant predictors might depend on the timing of the survey dates (e.g. snow
 650 accumulation vs. melt periods). Physical factors controlling the amount of absorbed sunlight
 651 such as shadow hours, aspect, and TCI may not be dominant in the early snow season because
 652 shortwave fluxes would have a cumulative effect on snow physical properties (Pomeroy and
 653 Brun, 2001). It is possible that spatial differences in absorbed solar energy have little control
 654 over snow depth variability because this analysis was performed early in the winter season and
 655 shortly after snowfall. To fully address this possibility, a similar analysis with a times series
 656 which tracks the snowpack evolution from the start of the accumulation season through the end
 657 of the ablation season is needed. In addition to high-resolution snow depth maps from a UAS-
 658 based lidar, albedo maps from a UAS-based visible and/or infrared sensor would be beneficial to
 659 improve the MaxEnt analysis by offering an accurate calculation of the absorbed radiative fluxes
 660 (Levy et al., 2018; Wang et al., 2020).

661 Due to the limited availability of soil data, we used the POLARIS soil data with relatively
 662 courser spatial resolution (30-m). Assuming that the soil data can represent spatial variability of
 663 the soil characteristics within the 830,000 m² study area, they were used as predictor variables in
 664 the MaxEnt framework and found as important variables. However, the courser spatial resolution
 665 could limit the confidence in the role of the soil variables in the MaxEnt. General evaluation of
 666 the POLARIS data against in-situ measurements provides r² values of 0.42 (Chaney et al., 2019).
 667 Additional validation against sample measurements in the study area may enhance the reliability
 668 of the MaxEnt model. Also, future research including supporting data such as soil and snow

669 temperature and/or snowmelt maps is also needed to fully address the role of spatially distributed
 670 soil properties in determining the spatial heterogeneity of energy transfer between the soil and
 671 the snowpack.

672 While the current results correspond to relatively flat terrain with low relief and a shallow
 673 snowpack, there is a possibility that the MaxEnt framework for different plant functional types,
 674 climate zones and/or snow classes could generate different results because previous studies
 675 indicate that snow depth patterns are largely affected by terrain characteristics and snow regimes
 676 (Anderton et al., 2004; Clark et al., 2011; Currier and Lundquist, 2018). Thus, as more high
 677 resolution snow depth data sets in different environments become available, it would be valuable
 678 to use the MaxEnt framework to better understand the spatial variability of snow depth. Lastly,
 679 the inclusion of relevant meteorological variables (e.g. solar radiation and wind speed/direction)
 680 in the MaxEnt is expected to provide a more robust determination of the dominant drivers among
 681 both static and dynamic variables. Application of the MaxEnt framework in a wide range of
 682 environments could potentially refine the parameterization of snowpack evolution in land surface
 683 models and down-scaling of remotely sensed snow products.

684 **6. Conclusion**

685 Understanding the spatial variability of snow is valuable for hydrologists and ecologists
 686 seeking to predict hydrological processes, species distributions, land-atmosphere interactions.
 687 However, identifying dominant physical drivers controlling the spatial structure of snow depth
 688 has been challenged due to the lack of high-resolution snowpack and physical variables with
 689 high vertical accuracy as well as limitations in traditional approaches. To overcome this, we first
 690 employ the MaxEnt framework with 1-m spatial snow and terrain maps from a UAS-based lidar
 691 system to identify physical variables controlling field-scale spatial structures of shallow,
 692 ephemeral snow depth over open terrain and forests. We found that, among the nine terrain, plant
 693 functional type, and soil variables, plant functional type and roughness had an important
 694 contribution in the MaxEnt framework as needed to predict spatial locations having either deeper
 695 or shallower snow depth across the landscape. Soil organic matter and saturated hydraulic
 696 conductivity were revealed as important controls on snow depth spatial variations for both fields
 697 and forest, suggesting spatial variations in the soil variables under the snowpack can control
 698 thermal transfer between soil and snowpack along with the near-surface atmosphere. Despite the

699 difference in controls and locations of the relatively shallow and deep snowpacks, the transition
 700 zones between areas with similar snow depths, as identified using local gradients, were
 701 consistent for both dates and well-characterized by the underlying local gradients of baseline
 702 flights without snow. It is expected that the results provide insight into snow and land surface
 703 models by aiding in the parameterization at the sub-grid scale and helping to support the down-
 704 scaling of retrieved remotely sensed snow products to characterize field-scale conditions.

705 Data Availability Statement

706 The UAS snow depth maps with topographic input variables from this study are available
 707 for download at [*will add link to data from Hydroshare, currently being setup with an ODC*
 708 *Attribution (ODC-BY) license for access without restrictions*]. POLARIS Soil property data used
 709 in this study are available from Chaney et al. (2019), respectively.

710 Acknowledgments

711 This study is based upon work supported by the Broad Agency Announcement Program
 712 and the U.S. Army Engineer Research and Development Center's Cold Region Research and
 713 Engineering Laboratory (ERDC-CRREL) under contract number W913E5-18-C-005. Any
 714 opinions, findings, and conclusions or recommendations in this material are those of the
 715 author(s) and do not necessarily reflect the views of the Broad Agency Announcement Program
 716 and the ERDC-CRREL. The authors are grateful to Christina Herrick for helping data collection
 717 and providing valuable comments.

718

719 References

- 720 Aanderud, Z. T., Jones, S. E., Schoolmaster Jr, D. R., Fierer, N., and Lennon, J. T. (2013).
 721 Sensitivity of soil respiration and microbial communities to altered snowfall, *Soil Biology*
 722 and *Biochemistry*, 57, 217-227.
- 723 Aase, J. K. and Siddoway, F. H.: Crown-Depth Soil Temperatures and Winter Protection for
 724 Winter Wheat Survival, *Soil Science Society of America Journal*, 43, 1229-1233, 1979.
- 725 Abu-Hamdeh, N. H., & Reeder, R. C. (2000). Soil thermal conductivity effects of density,
 726 moisture, salt concentration, and organic matter. *Soil science society of America*
 727 *Journal*, 64(4), 1285-1290.
- 728 Algeo, T. P., Slate, D., Caron, R. M., Atwood, T., Recuenco, S., Ducey, M. J., ... & Palace, M.
 729 (2017). Modeling raccoon (*Procyon lotor*) habitat connectivity to identify potential
 730 corridors for rabies spread. *Tropical medicine and infectious disease*, 2(3), 44.

- 731 Anderton, S. P. (2000). An analysis of spatial variability in snow processes in a high mountain
 732 catchment, *Doctoral dissertation, University of Durham*.
- 733 Anderton, S. P., White, S. M., & Alvera, B. (2002). Micro-scale spatial variability and the timing
 734 of snow melt runoff in a high mountain catchment. *Journal of Hydrology*, 268(1-4), 158-
 735 176.
- 736 Anderton, S. P., White, S. M., & Alvera, B. (2004). Evaluation of spatial variability in snow
 737 water equivalent for a high mountain catchment. *Hydrological Processes*, 18(3), 435-453.
- 738 Arnold, N. S., & Rees, W. G. (2003). Self-similarity in glacier surface characteristics. *Journal of*
 739 *Glaciology*, 49(167), 547-554.
- 740 Baldwin, R. A. (2009). Use of maximum entropy modeling in wildlife research. *Entropy*, 11(4),
 741 854-866.
- 742 Barnett, T. P., Adam, J. C., & Lettenmaier, D. P. (2005). Potential impacts of a warming climate
 743 on water availability in snow-dominated regions. *Nature*, 438(7066), 303-309.
- 744 Blöschl, G., & Kirnbauer, R. (1992). An analysis of snow cover patterns in a small alpine
 745 catchment. *Hydrological Processes*, 6(1), 99-109.
- 746 Booker, D. J., & Woods, R. A. (2014). Comparing and combining physically-based and
 747 empirically-based approaches for estimating the hydrology of ungauged
 748 catchments. *Journal of Hydrology*, 508, 227-239.
- 749 Broxton, P. D., Van Leeuwen, W. J., & Biederman, J. A. (2019). Improving snow water
 750 equivalent maps with machine learning of snow survey and lidar measurements. *Water*
 751 *Resources Research*, 55(5), 3739-3757.
- 752 Burakowski, E., and Hamilton. L., (2020). Are New Hampshire's Winters Warming? Yes, but
 753 fewer than half state residents recognize the trend. Regional Issue Brief #61. Carsey
 754 School of Public Policy, University of New Hampshire.
 755 <https://dx.doi.org/10.34051/p/2020.377>
- 756 Burakowski, E., Tawfik, A., Ouimette, A., Lepine, L., Novick, K., Ollinger, S., ... & Bonan, G.
 757 (2018). The role of surface roughness, albedo, and Bowen ratio on ecosystem energy
 758 balance in the Eastern United States. *Agricultural and Forest Meteorology*, 249, 367-376.
- 759 Burakowski, E., Wake, C. P., Dibb, J. E., & Stampone, M. (2013). Putting the capital 'A'in
 760 CoCoRAHS: an experimental programme to measure albedo using the Community
 761 Collaborative Rain, Hail & Snow (CoCoRaHS) Network. *Hydrological Processes*, 27(21),
 762 3024-3034.
- 763 Carroll, R. W., Deems, J. S., Niswonger, R., Schumer, R., & Williams, K. H. (2019). The
 764 importance of interflow to groundwater recharge in a snowmelt-dominated headwater
 765 basin. *Geophysical Research Letters*, 46(11), 5899-5908.
- 766 Chaney, N. W., Minasny, B., Herman, J. D., Nauman, T. W., Brungard, C. W., Morgan, C. L., ...
 767 & Yimam, Y. (2019). POLARIS soil properties: 30-m probabilistic maps of soil
 768 properties over the contiguous United States. *Water Resources Research*, 55(4), 2916-
 769 2938.
- 770 Chaney, N. W., Wood, E. F., McBratney, A. B., Hempel, J. W., Nauman, T. W., Brungard, C.
 771 W., & Odgers, N. P. (2016). POLARIS: A 30-meter probabilistic soil series map of the
 772 contiguous United States. *Geoderma*, 274, 54-67.
- 773 Cho, E., Jacobs, J. M., & Vuyovich, C. M. (2020). The value of long-term (40 years) airborne
 774 gamma radiation SWE record for evaluating three observation-based gridded SWE data
 775 sets by seasonal snow and land cover classifications. *Water Resources Research*, 56(1),
 776 e2019WR025813.

- 777 Clark, M. P., Hendrikx, J., Slater, A. G., Kavetski, D., Anderson, B., Cullen, N. J., ... & Woods,
 778 R. A. (2011). Representing spatial variability of snow water equivalent in hydrologic and
 779 land-surface models: A review. *Water Resources Research*, 47(7).
- 780 Cline, D., Yueh, S., Chapman, B., Stankov, B., Gasiewski, A., Masters, D., Elder, K., Kelly, R.,
 781 Painter, T. H., Miller, S., Katzberg, S., & Mahrt, L. (2009). NASA Cold Land Processes
 782 Experiment (CLPX 2002/03): Airborne Remote Sensing. *Journal of Hydrometeorology*,
 783 10, 338–346. <http://dx.doi.org/10.1175/2008JHM883.1>.
- 784 Currier, W. R., & Lundquist, J. D. (2018). Snow depth variability at the forest edge in multiple
 785 climates in the western United States. *Water Resources Research*, 54(11), 8756-8773.
- 786 Cutler, D. R., Edwards Jr, T. C., Beard, K. H., Cutler, A., Hess, K. T., Gibson, J., & Lawler, J. J.
 787 (2007). Random forests for classification in ecology. *Ecology*, 88(11), 2783-2792.
- 788 DeBeer, C. M., & Pomeroy, J. W. (2010). Simulation of the snowmelt runoff contributing area in
 789 a small alpine basin. *Hydrology and Earth System Sciences*, 14(7), 1205.
- 790 Deems, J. S., Fassnacht, S. R., & Elder, K. J. (2006). Fractal distribution of snow depth from
 791 LiDAR data. *Journal of Hydrometeorology*, 7(2), 285-297.
- 792 Deems, J. S., Painter, T. H., & Finnegan, D. C. (2013). Lidar measurement of snow depth: a
 793 review. *Journal of Glaciology*, 59(215), 467-479.
- 794 Derksen, C., Toose, P., Rees, A., Wang, L., English, M., Walker, A., & Sturm, M. (2010).
 795 Development of a tundra-specific snow water equivalent retrieval algorithm for satellite
 796 passive microwave data. *Remote Sensing of Environment*, 114(8), 1699–1709.
 797 <https://doi.org/10.1016/j.rse.2010.02.019>
- 798 Djebou, D. C. S., & Singh, V. P. (2015). Retrieving vegetation growth patterns from soil
 799 moisture, precipitation and temperature using maximum entropy. *Ecological
 800 Modelling*, 309, 10-21.
- 801 Dudik M, Phillips S, Schapire R (2007) Maximum entropy density estimation with generalized
 802 regularization and an application to species distribution modeling. *Journal of Machine
 803 Learning Research*, 8(6):1217–1260.
- 804 Earman, S., Campbell, A. R., Phillips, F. M., & Newman, B. D. (2006). Isotopic exchange
 805 between snow and atmospheric water vapor: Estimation of the snowmelt component of
 806 groundwater recharge in the southwestern United States. *Journal of Geophysical
 807 Research: Atmospheres*, 111(D9).
- 808 Essery, R.L., Bunting, P., Hardy, J. Link, T., Marks, D., Melloh, R., Pomeroy, J., Rowlands, A.,
 809 and Rutter., N. (2008). Radiative transfer modeling of a coniferous canopy characterized
 810 by airborne remote sensing. *Journal of Hydrometeorology*, 9: 228–241.
- 811 Elith J, et al. (2006) Novel methods improve prediction of species' distributions from occurrence
 812 data. *Ecography* (Cop.) 29(2):129–151.
- 813 Farouki, O. T. (1981). The thermal properties of soils in cold regions. *Cold Regions Science and
 814 Technology*, 5(1), 67-75.
- 815 Fey, C., Schattan, P., Helffricht, K., & Schöber, J. (2019). A compilation of multitemporal TLS
 816 snow depth distribution maps at the Weisssee snow research site (Kaunertal,
 817 Austria). *Water Resources Research*, 55(6), 5154-5164.
- 818 Fey, C., & Wichmann, V. (2017). Long-range terrestrial laser scanning for geomorphological
 819 change detection in alpine terrain—handling uncertainties. *Earth Surface Processes and
 820 Landforms*, 42(5), 789-802.

- 821 Fischer, S., Bühler, P., Büttner, U., & Schumann, A. (2020). The use of maximum entropy to
 822 increase the informational content of hydrological networks by additional
 823 gauges. *Hydrological Sciences Journal*, 65(13), 2274-2285.
- 824 Ge, Y., & Gong, G. (2010). Land surface insulation response to snow depth variability. *Journal*
 825 *of Geophysical Research: Atmospheres*, 115(D8).
- 826 Gelfan, A. N., Pomeroy, J. W., & Kuchment, L. S. (2004). Modeling forest cover influences on
 827 snow accumulation, sublimation, and melt. *Journal of Hydrometeorology*, 5(5), 785-803.
- 828 Goetz, J., & Brenning, A. (2019). Quantifying uncertainties in snow depth mapping from
 829 structure from motion photogrammetry in an alpine area. *Water Resources*
 830 *Research*, 55(9), 7772-7783.
- 831 Gray, D. M., & Male, D. H. (1981). Handbook of snow: Principles, processes, management and
 832 use. Toronto: Pergamon Press.
- 833 Grayson, R. B., Blöschl, G., Western, A. W., & McMahon, T. A. (2002). Advances in the use of
 834 observed spatial patterns of catchment hydrological response. *Advances in Water*
 835 *Resources*, 25(8-12), 1313-1334.
- 836 Groffman, P. M., Driscoll, C. T., Fahey, T. J., Hardy, J. P., Fitzhugh, R. D., & Tierney, G. L.
 837 (2001). Colder soils in a warmer world: a snow manipulation study in a northern
 838 hardwood forest ecosystem. *Biogeochemistry*, 56(2), 135-150.
- 839 Grünewald, T., and M. Lehning (2011), Altitudinal dependency of snow amounts in two small
 840 alpine catchments: Can catchment-wide snow amounts be estimated via single snow or
 841 precipitation stations, *Annals of Glaciology*, 52(58), 153–158,
 842 doi:10.3189/172756411797252248.
- 843 Harder, P., Pomeroy, J. W., & Helgason, W. (2017). Local-scale advection of sensible and latent
 844 heat during snowmelt. *Geophysical Research Letters*, 44(19), 9769-9777.
- 845 Harder, P., Pomeroy, J. W., & Helgason, W. D. (2020). Improving sub-canopy snow depth
 846 mapping with unmanned aerial vehicles: lidar versus structure-from-motion
 847 techniques. *The Cryosphere*, 14(6), 1919-1935.
- 848 Harpold, A. A., Guo, Q., Molotch, N., Brooks, P. D., Bales, R., Fernandez-Diaz, J. C., ... &
 849 Flanagan, J. (2014). LiDAR-derived snowpack data sets from mixed conifer forests
 850 across the Western United States. *Water Resources Research*, 50(3), 2749-2755.
- 851 Harpold, A. A., Molotch, N. P., Musselman, K. N., Bales, R. C., Kirchner, P. B., Litvak, M., &
 852 Brooks, P. D. (2015). Soil moisture response to snowmelt timing in mixed-conifer
 853 subalpine forests. *Hydrological Processes*, 29(12), 2782-2798.
- 854 He, X., Chaney, N. W., Schleiss, M., & Sheffield, J. (2016). Spatial downscaling of precipitation
 855 using adaptable random forests. *Water Resources Research*, 52(10), 8217-8237.
- 856 Henry, H. A. L. (2008). Climate change and soil freezing dynamics: historical trends and
 857 projected changes, *Climatic Change*, 87, 421-434.
- 858 Hojatimalekshah, A., Uhlmann, Z., Glenn, N. F., Hiemstra, C. A., Tennant, C. J., Graham, J.
 859 D., ... & Enterkine, J. (2020). Tree canopy and snow depth relationships at fine scales
 860 with terrestrial laser scanning. *The Cryosphere Discussions*, 1-35.
 861 <https://doi.org/10.5194/tc-2020-277>
- 862 Horn, B.K.P. (1981). Hill shading and the reflectance map. *Proceedings of the IEEE*, 69(1): 14-
 863 47. Doi: 10.1109/PROC.1981.11918.
- 864 Howey, M. C., Palace, M. W., & McMichael, C. H. (2016). Geospatial modeling approach to
 865 monument construction using Michigan from AD 1000–1600 as a case
 866 study. *Proceedings of the National Academy of Sciences*, 113(27), 7443-7448.

- 867 Huerta, M.L, Molotch, N.P., and McPhee. J., (2019). Snowfall interception in a deciduous
 868 Nothofagus forest and implications for spatial snowpack distribution. *Hydrological
 869 Processes*, 33(13): 1818-1834.
- 870 Isard, S. A., & Schaetzl, R. J. (1998). Effects of winter weather conditions on soil freezing in
 871 southern Michigan. *Physical Geography*, 19(1), 71-94.
- 872 Jacobs, J. M., Hunsaker, A. G., Sullivan, F. B., Palace, M., Burakowski, E. A., Herrick, C., &
 873 Cho, E. (2021). Shallow snow depth mapping with unmanned aerial systems lidar
 874 observations: A case study in Durham, New Hampshire, United States. *The Cryosphere*,
 875 15, 1-17, <https://doi.org/10.5194/tc-2020-37>.
- 876 Jaynes E. T. (1957) Information theory and statistical mechanics. *Physical Review*. 106(4):620–
 877 630.
- 878 Keum, J., Coulibaly, P., Razavi, T., Tapsoba, D., Gobena, A., Weber, F., & Pietroniro, A. (2018).
 879 Application of SNODAS and hydrologic models to enhance entropy-based snow
 880 monitoring network design. *Journal of Hydrology*, 561, 688-701.
- 881 Kirchner, P. B., Bales, R. C., Molotch, N. P., Flanagan, J., & Guo, Q. (2014). LiDAR
 882 measurement of seasonal snow accumulation along an elevation gradient in the southern
 883 Sierra Nevada, California. *Hydrology & Earth System Sciences*, 18(10).
- 884 Lapena, D. R., & Martz, L. W. (1996). An investigation of the spatial association between snow
 885 depth and topography in a Prairie agricultural landscape using digital terrain
 886 analysis. *Journal of Hydrology*, 184(3-4), 277-298.
- 887 Lawrence, D. M., & Slater, A. G. (2010). The contribution of snow condition trends to future
 888 ground climate. *Climate dynamics*, 34(7-8), 969-981.
- 889 Lehning, M., Grünwald, T., & Schirmer, M. (2011). Mountain snow distribution governed by
 890 an altitudinal gradient and terrain roughness. *Geophysical Research Letters*, 38(19).
- 891 Lemmettyinen, J., Derksen, C., Rott, H., Macelloni, G., King, J., Schneebeli, M., Wiesmann, A.,
 892 Leppänen, L., Kontu, A. and Pullainen, J., (2018). Retrieval of effective correlation
 893 length and snow water equivalent from radar and passive microwave measurements.
 894 *Remote Sensing*, 10(2), 170.
- 895 Levy, C. R., Burakowski, E., & Richardson, A. D. (2018). Novel measurements of fine-scale
 896 albedo: Using a commercial quadcopter to measure radiation fluxes. *Remote
 897 Sensing*, 10(8), 1303.
- 898 Liston, G. E. (1999). Interrelationships among snow distribution, snowmelt, and snow cover
 899 depletion: Implications for atmospheric, hydrologic, and ecologic modeling. *Journal of
 900 applied meteorology*, 38(10), 1474-1487.
- 901 López-Moreno, J. I., & Nogués-Bravo, D. (2005). A generalized additive model for the spatial
 902 distribution of snowpack in the Spanish Pyrenees. *Hydrological Processes: An
 903 International Journal*, 19(16), 3167-3176.
- 904 López-Moreno, J. I., Revuelto, J., Alonso-González, E., Sanmiguel-Vallelado, A., Fassnacht, S.
 905 R., Deems, J., & Morán-Tejeda, E. (2017). Using very long-range terrestrial laser scanner
 906 to analyze the temporal consistency of the snowpack distribution in a high mountain
 907 environment. *Journal of Mountain Science*, 14(5), 823-842.
- 908 Luce, C. H., Tarboton, D. G., & Cooley, K. R. (1999). Sub-grid parameterization of snow
 909 distribution for an energy and mass balance snow cover model. *Hydrological
 910 Processes*, 13(12-13), 1921-1933.

- 911 Lundquist, J. D., Cayan, D. R., & Dettinger, M. D. (2004). Spring onset in the Sierra Nevada:
 912 When is snowmelt independent of elevation?. *Journal of Hydrometeorology*, 5(2), 327-
 913 342.
- 914 Lundquist, J. E., Dickerson-Lange, S.E. Lutz, J.A. and Cristea., N.C. (2013). Lower forest
 915 density enhances snow retention in regions with warmer winters: a global framework
 916 developed from plot-scale observations and modeling, *Water Resources Research*, 49:
 917 6356–6370, <https://doi.org/10.1002/wrcr.20504>, 2013.
- 918 Mazzotti, G., Currier, W. R., Deems, J. S., Pflug, J. M., Lundquist, J. D., & Jonas, T. (2019).
 919 Revisiting snow cover variability and canopy structure within forest stands: Insights from
 920 airborne lidar data. *Water Resources Research*, 55(7), 6198-6216.
- 921 Maurer, G. E., & Bowling, D. R. (2014). Seasonal snowpack characteristics influence soil
 922 temperature and water content at multiple scales in interior western US mountain
 923 ecosystems. *Water Resources Research*, 50(6), 5216-5234.
- 924 McMichael, C. H., Palace, M. W., & Golightly, M. (2014). Bamboo-dominated forests and
 925 pre-Columbian earthwork formations in south-western Amazonia. *Journal of
 926 Biogeography*, 41(9), 1733-1745.
- 927 McNay, R.S., Peterson, L.D., and Nyberg., J.B. (1988). The influence of forest stand
 928 characteristics on snow interception in the coastal forests of British Columbia. *Canadian
 929 Journal of Forest Resources*, 18: 566-573.
- 930 Merow, C., Smith, M. J., & Silander Jr, J. A. (2013). A practical guide to MaxEnt for modeling
 931 species' distributions: what it does, and why inputs and settings
 932 matter. *Ecography*, 36(10), 1058-1069.
- 933 Mishra, A. K., & Coulibaly, P. (2009). Developments in hydrometric network design: A
 934 review. *Reviews of Geophysics*, 47(2).
- 935 Mohanty, B. P., Klittich, W. M., Horton, R., & Van Genuchten, M. T. (1995). Spatio-temporal
 936 variability of soil temperature within three land areas exposed to different tillage
 937 systems. *Soil Science Society of America Journal*, 59(3), 752-759.
- 938 Monson, R. K., Lipson, D. L., Burns, S. P., Turnipseed, A. A., Delany, A. C., Williams, M. W.,
 939 and Schmidt, S. K. (2006). Winter forest soil respiration controlled by climate and
 940 microbial community composition, *Nature*, 439, 711.
- 941 Mott, R., Schirmer, M., & Lehning, M. (2011). Scaling properties of wind and snow depth
 942 distribution in an Alpine catchment. *Journal of Geophysical Research: Atmospheres*, 116(D6).
- 943 Mott, R., Gromke, C., Grünwald, T., & Lehning, M. (2013). Relative importance of advective
 944 heat transport and boundary layer decoupling in the melt dynamics of a patchy snow
 945 cover. *Advances in Water Resources*, 55, 88–97.
 946 <https://doi.org/10.1016/j.advwatres.2012.03.001>
- 947 Musselman, K., Molotch, N.P., and Brooks., P.D. (2008). Effects of vegetation on snow
 948 accumulation and ablation in a mid-latitude sub-alpine forest. *Hydrological Processes*, 22:
 949 2767-2776., doi:10.1002/hyp.7050.
- 950 Nakai, Y., Kitahara, H., Sakamoto, T., Saito, T., and Terajima. T., (1993). Evaporation of snow
 951 intercepted by forest canopies. *Journal of Japan Forest Society*, 75: 191-200 (in Japanese
 952 with English summary).
- 953 New Hampshire State Climate Office (2014). Climate normals (1981-2010) for selected NH
 954 cities and towns. www.unh.edu/stateclimatologist/nhnormals.html

- 956 Ng, A. Y., & Jordan, M. I. (2002). On discriminative vs. generative classifiers: A comparison of
 957 logistic regression and naive bayes. In *Advances in neural information processing*
 958 *systems* (pp. 841-848).
- 959 Painter, T. H., Berisford, D. F., Boardman, J. W., Bormann, K. J., Deems, J. S., Gehrke, F., ... &
 960 Mattmann, C. (2016). The Airborne Snow Observatory: Fusion of scanning lidar,
 961 imaging spectrometer, and physically-based modeling for mapping snow water
 962 equivalent and snow albedo. *Remote Sensing of Environment*, 184, 139-152.
- 963 Palace, M. W., McMichael, C. N. H., Braswell, B. H., Hagen, S. C., Bush, M. B., Neves, E., ... &
 964 Frolking, S. (2017). Ancient Amazonian populations left lasting impacts on forest
 965 structure. *Ecosphere*, 8(12), e02035.
- 966 Parikh, R. J., Havens, J. A., & Scott, H. D. (1979). Thermal diffusivity and conductivity of moist
 967 porous media. *Soil Science Society of America Journal*, 43(5), 1050-1052.
- 968 Penner, E. (1970). Thermal conductivity of frozen soils. *Canadian Journal of Earth
 969 Sciences*, 7(3), 982-987.
- 970 Perron, C.J., Bennett, K., & Lee, T.D. (2004). Forest stewardship plan: Thompson farm. NH:
 971 University of New Hampshire. Produced by Ossipee Mountain Land Company, West
 972 Ossipee, <https://colsa.unh.edu/sites/default/files/thompson-farm-plan.pdf>.
- 973 Peters, J., De Baets, B., Verhoest, N. E., Samson, R., Degroeve, S., De Becker, P., & Huybrechts,
 974 W. (2007). Random forests as a tool for ecohydrological distribution
 975 modelling. *Ecological Modelling*, 207(2-4), 304-318.
- 976 Phillips, S. J., Dudík, M., & Schapire, R. E. (2004). A maximum entropy approach to species
 977 distribution modeling. In *Proceedings of the twenty-first international conference on
 978 Machine learning* (p. 83).
- 979 Phillips, S. J., Anderson, R. P., & Schapire, R. E. (2006). Maximum entropy modeling of species
 980 geographic distributions. *Ecological modelling*, 190(3-4), 231-259.
- 981 Phillips, S., & Dudík, M. (2008) Modeling of species distributions with Maxent: New extensions
 982 and a comprehensive evaluation. *Ecography* (Cop.) 31(2):161–175.
- 983 Pflug, J. M., & Lundquist, J. D. (2020). Inferring distributed snow depth by leveraging snow
 984 pattern repeatability: Investigation using 47 lidar observations in the Tuolumne watershed,
 985 Sierra Nevada, California. *Water Resources Research*, 56(9), e2020WR027243.
- 986 Pomeroy, J. W., & Brun, E. (2001). Physical properties of snow. Snow ecology: An
 987 interdisciplinary examination of snow-covered ecosystems, 45, 118.
- 988 Pomeroy, J.W. and Gray. D.M. (1995). Snowcover accumulation, relocation, and management.
 989 National Hydrology Research Institute Science Report No. 7. Hydrological Sciences
 990 Division, NHRI, Division of Hydrology, University of Saskatchewan. Environment
 991 Canada.
- 992 Pomeroy, J. W., Gray, D. M., Shook, K. R., Toth, B., Essery, R. L. H., Pietroniro, A., &
 993 Hedstrom, N. (1998). An evaluation of snow accumulation and ablation processes for
 994 land surface modelling. *Hydrological Processes*, 12(15), 2339-2367.
- 995 Prokop, A. (2008). Assessing the applicability of terrestrial laser scanning for spatial snow depth
 996 measurements. *Cold Regions Science and Technology*, 54(3), 155-163.
- 997 Rahmati, O., Pourghasemi, H. R., & Melesse, A. M. (2016). Application of GIS-based data
 998 driven random forest and maximum entropy models for groundwater potential mapping:
 999 a case study at Mehran Region, Iran. *Catena*, 137, 360-372.
- 1000 Redding, T., & Devito, K. (2011). Aspect and soil textural controls on snowmelt runoff on
 1001 forested Boreal Plain hillslopes. *Hydrology Research*, 42(4), 250-267.

- 1002 Reinmann, A. B. and Templer, P. H.: Increased soil respiration in response to experimentally
 1003 reduced snow cover and increased soil freezing in a temperate deciduous forest,
 1004 *Biogeochemistry*, 140, 359-371, 2018.
- 1005 Revuelto, J., López-Moreno, J. I., Azorin-Molina, C., & Vicente-Serrano, S. M. (2014).
 1006 Topographic control of snowpack distribution in a small catchment in the central Spanish
 1007 Pyrenees: intra-and inter-annual persistence. *The Cryosphere*, 8(5), 1989-2006.
- 1008 Roth, T.R. and Nolin. A.W. (2017). Forest impacts on snow accumulation and ablation across
 1009 and elevation gradient in a temperate montane environment. *Hydrology and Earth System
 1010 Sciences*, 21: 5427-5442, <https://doi.org/10.5194/hess-21-5427-2017>.
- 1011 Saberi, N., Kelly, R., Flemming, M., & Li, Q. (2020). Review of snow water equivalent retrieval
 1012 methods using spaceborne passive microwave radiometry. *International Journal of
 1013 Remote Sensing*, 41(3), 996-1018.
- 1014 Sanders-DeMott, R., Ouimette, A. P., Lepine, L. C., Fogarty, S. Z., Burakowski, E. A., Contosta,
 1015 A. R., & Ollinger, S. V. (2020). Divergent carbon cycle response of forest and
 1016 grass-dominated northern temperate ecosystems to record winter warming. *Global
 1017 Change Biology*, 26(3), 1519-1531.
- 1018 Schlägl, S., Lehning, M., & Mott, R. (2018). How are turbulent sensible heat fluxes and snow
 1019 melt rates affected by a changing snow cover fraction?. *Frontiers in Earth Science*, 6,
 1020 154.
- 1021 Schmidt, R.A. and D.R. Gluns. (1991) Snowfall interception on branches of three conifer species.
 1022 *Canadian Journal of Forest Research*, 21:1262-1269.
- 1023 Schirmer, M., & Lehning, M. (2011). Persistence in intra-annual snow depth distribution: 2.
 1024 Fractal analysis of snow depth development. *Water Resources Research*, 47(9).
- 1025 Schirmer, M., & Pomeroy, J. W. (2020). Processes governing snow ablation in alpine terrain—
 1026 detailed measurements from the Canadian Rockies. *Hydrology and Earth System
 1027 Sciences*, 24(1), 143-157.
- 1028 Shook, K., Gray, D. M., & Pomeroy, J. W. (1993). Temporal Variation in Snowcover Area
 1029 During Melt in Prairie and Alpine Environments: Paper presented at the 9th Northern Res.
 1030 Basin Symposium/Workshop (Whitehorse/Dawson/Inuvik, Canada-August
 1031 1992). *Hydrology Research*, 24(2-3), 183-198.
- 1032 Singh, V. P. (1997). The use of entropy in hydrology and water resources. *Hydrological
 1033 processes*, 11(6), 587-626.
- 1034 Sorensen, P. O., Finzi, A. C., Giasson, M.-A., Reinmann, A. B., Sanders-DeMott, R., and
 1035 Templer, P. H. (2018). Winter soil freeze-thaw cycles lead to reductions in soil microbial
 1036 biomass and activity not compensated for by soil warming, *Soil Biology and
 1037 Biochemistry*, 116, 39-47.
- 1038 Sørensen, R., Zinko, U., and Seibert, J. (2006). On the calculation of the topographic wetness
 1039 index: evaluation of different methods based on field observations, *Hydrology and Earth
 1040 System Sciences*, 10, 101–112, <https://doi.org/10.5194/hess-10-101-2006>.
- 1041 Starkloff, T., Stolte, J., Hessel, R., and Ritsema, C.: Investigating the development of shallow
 1042 snowpacks on arable land, using comprehensive field observations and spatially
 1043 distributed snow modelling, *Hydrology Research*, 49, 41-59, 2017.
- 1044 Stieglitz, M., Ducharme, A., Koster, R., & Suarez, M. (2001) The impact of detailed snow
 1045 physics on the simulation of snow cover and subsurface thermodynamics at continental
 1046 scales. *Journal of Hydrometeorology*, 2(3), 228-242.

- 1047 Storck, P., Lettenmaier, D.P. and Bolton. S.M. (2002) Measurement of snow interception and
 1048 canopy effects on snow accumulation and melt in a mountainous maritime climate,
 1049 Oregon, United States. *Water Resources Research*, 38(11): 1223. <https://doi.org/10.1029/2002WR001281>
- 1050 Sturm, M., Goldstein, M. A., & Parr, C. (2017). Water and life from snow: A trillion dollar
 1051 science question. *Water Resources Research*, 53(5), 3534-3544.
- 1052 Sturm, M., & Holmgren, J. (2018). An automatic snow depth probe for field validation
 1053 campaigns. *Water Resources Research*, 54(11), 9695-9701.
- 1054 Sturm, M., & Wagner, A. M. (2010). Using repeated patterns in snow distribution modeling: An
 1055 Arctic example. *Water Resources Research*, 46, W12549.
- 1056 Tinkham, W. T., Smith, A. M., Marshall, H. P., Link, T. E., Falkowski, M. J., & Winstral, A. H.
 1057 (2014). Quantifying spatial distribution of snow depth errors from LiDAR using Random
 1058 Forest. *Remote sensing of environment*, 141, 105-115.
- 1059 Trujillo, E., Ramírez, J. A., & Elder, K. J. (2007). Topographic, meteorologic, and canopy
 1060 controls on the scaling characteristics of the spatial distribution of snow depth
 1061 fields. *Water Resources Research*, 43(7).
- 1062 Tucker, C. L., Tamang, S., Pendall, E., and Ogle, K. (2016). Shallow snowpack inhibits soil
 1063 respiration in sagebrush steppe through multiple biotic and abiotic mechanisms,
 1064 *Ecosphere*, 7, e01297.
- 1065 Yi, Y., Kimball, J. S., Chen, R. H., Moghaddam, M., and Miller, C. E. (2019). Sensitivity of
 1066 active-layer freezing process to snow cover in Arctic Alaska, *The Cryosphere*, 13, 197.
- 1067 Wang, J., & Bras, R. L. (2011). A model of evapotranspiration based on the theory of maximum
 1068 entropy production. *Water Resources Research*, 47(3).
- 1069 Wang, W., Yang, K., Zhao, L., Zheng, Z., Lu, H., Mamtimin, A., ... & Moore, J. C. (2020).
 1070 Characterizing surface albedo of shallow fresh snow and its importance for snow ablation
 1071 on the interior of the Tibetan Plateau. *Journal of Hydrometeorology*, 21(4), 815-827.
- 1072 Westhoff, M. C., Zehe, E., & Schymanski, S. J. (2014). Importance of temporal variability for
 1073 hydrological predictions based on the maximum entropy production
 1074 principle. *Geophysical Research Letters*, 41(1), 67-73.
- 1075 Zehe, E., Blume, T., & Blöschl, G. (2010). The principle of ‘maximum energy dissipation’: a
 1076 novel thermodynamic perspective on rapid water flow in connected soil
 1077 structures. *Philosophical Transactions of the Royal Society B: Biological
 1078 Sciences*, 365(1545), 1377-1386.
- 1079 Zhu, D., Ciais, P., Krinner, G., Maignan, F., Puig, A. J., & Hugelius, G. (2019). Controls of soil
 1080 organic matter on soil thermal dynamics in the northern high latitudes. *Nature
 1081 communications*, 10(1), 1-9.
- 1082

1083 Highlights

- 1084 • Drivers of snow spatial patterns from UAS lidar were identified using MaxEnt
 1085 • Plant functional type and terrain roughness are the largest contributors
 1086 • Soil properties were also important controls probably due to thermal transfer

1087
 1088
 1089 **Eunsang Cho:** Conceptualization, Methodology, Writing- Original draft

1090 preparation, Visualization, **Adam G. Hunsaker:** Data Curation, Visualization, Writing - Review

1091 & Editing, **Jennifer Jacobs**: Supervision, Conceptualization, Project administration, Funding
 1092 acquisition, Writing - Review & Editing, **Michael Palace**: Conceptualization, Methodology,
 1093 Writing - Review & Editing, **Franklin B. Sullivan**: Data Curation, Writing - Review & Editing,
 1094 **Elizabeth A. Burakowski**: Methodology, Writing - Review & Editing.
 1095

1096 **Abstract**

1097 Understanding the spatial variability of the snowpack is valuable for hydrologists and
 1098 ecologists seeking to predict hydrological processes in a cold region. Snow distribution is a
 1099 function of interactions among static variables, such as terrain, vegetation, and soil properties,
 1100 and dynamic meteorological variables, such as solar radiation, wind speed and direction, and soil
 1101 moisture. However, identifying the dominant physical drivers responsible for spatial patterns of
 1102 the snowpack, particularly for ephemeral, shallow snowpacks, has been challenged due to the
 1103 lack of the high-resolution snowpack and physical variables with high vertical accuracy as well
 1104 as inherent limitations in traditional approaches. This study uses an Unpiloted Aerial System
 1105 (UAS) lidar-based snow depth and static variables (1-m spatial resolution) to analyze field-scale
 1106 spatial structures of snow depth and apply the Maximum Entropy (MaxEnt) model to identify
 1107 primary controls over open terrain and forests at the University of New Hampshire Thompson
 1108 Farm Research Observatory, New Hampshire, United States. We found that, among nine
 1109 topographic and soil variables, plant functional type and terrain roughness contribute up to 80%
 1110 and 76% of relative importance in the MaxEnt framework to predicting locations of deeper or
 1111 shallower snowpacks, respectively, across a mixed temperate forested and field landscape. Soil
 1112 variables, such as organic matter and saturated hydraulic conductivity, were also important
 1113 controls (up to 70% and 81%) on snow depth spatial variations for both open and forested
 1114 landscapes suggesting spatial variations in soil variables under snow can control thermal transfer
 1115 among soil, snowpack, and surface-atmosphere. This work contributes to improving land surface
 1116 and snow models by informing parameterization of the sub-grid scale snow depths, down-scaling
 1117 remotely sensed snow products, and understanding field scale snow states.

1118
 1119